POLITECNICO DI TORINO

Master's Degree in Automotive Engineering

Politecnico
di Torino

Master's Degree Thesis

Numerical analysis of sloshing phenomenon in heavy-duty vehicles

Supervisors

Prof. Alessandro VIGLIANI

Prof. Enrico GALVAGNO

Prof. Angelo VELLA

Prof. Luca ZERBATO

Candidate

Giuseppe CAMPANA

December 2023

Abstract

Heavy-duty vehicles carrying liquids are subjected to higher instability than others due to sloshing phenomenon. In this case a vehicle composed by tractor and trailer is taken into account. When the tank is partially filled, the liquid tends to move, affecting the vehicle handling and stability. In this study the sloshing problem is analysed in Simscape environment, thanks to the *Simscape Vehicle Templates* model created by Steve Miller. The sloshing phenomenon have been represented with an equivalent mechanical model, in particular by means of pendulums. In order to run numerical simulations, sloshing parameters and functions have been written in *Matlab*. Moreover, to proper simulate real world, several manoeuvres have been considered. In this way transient and steady-state behaviours are analysed.

Table of Contents

List of Tables IV

List of Figures V

1 Introduction 1

2 Types of model 3
2.1 Equivalent mechanical models . . . 3
2.1.1 Mass-spring-damper model . . . 3
2.1.2 Simple pendulum model . . . 4
2.1.3 Trammel pendulum model . . . 6
2.2 Fluid-solid coupling system . . . 7

3 Lateral sloshing 9
3.1 Effects of different manoeuvres . . . 9
3.2 Overturning . . . 11
3.3 Analytical lateral model . . . 16
3.3.1 Rigid vehicle model . . . 16
3.3.2 Simple pendulum sloshing model . . . 19
3.3.3 Analytical model results . . . 23
3.3.4 *Simscape Vehicle Template* simulations . . . 24
3.3.5 Frequency analysis . . . 29

4 Longitudinal sloshing 37
4.1 Braking manoeuvre . . . 37
4.2 Equivalent mechanical model . . . 38
4.3 Model validation . . . 44
4.4 Jack-knife instability . . . 49
4.4.1 Jack-knife with lateral sloshing . . . 50
4.4.2 Jack-knife with longitudinal sloshing . . . 51

5 Conclusions 59

A Nomenclature 60

B Vehicle data for lateral sloshing 62
B.1 Tractor 62
B.2 Trailer 65

C Vehicle data for longitudinal sloshing 67
C.1 Tractor 67
C.2 Trailer 70

Bibliography 72

List of Tables

4.1 Mean longitudinal force at 0.3 g. 45
4.2 Amplification factor at 0.3 g. 47
4.3 Vehicle data used in simulation. 47

B.1 Main tractor parameters settings. 63
B.2 Tractor geometry parameters settings. 64
B.3 Tractor's tires settings. 64
B.4 Main trailer parameters settings. 65
B.5 Trailer geometry parameters settings. 66
B.6 Trailer's tires settings. 66

C.1 Main tractor parameters settings. 68
C.2 Tractor geometry parameters settings. 69
C.3 Main trailer parameters settings. 70
C.4 Trailer geometry parameters settings. 70

List of Figures

1.1 Example of lateral sloshing CFD simulation result, [2]. 2

2.1 Mass-spring-damper model (a), free surface of the liquid (b), [3]. . . 4
2.2 Scheme of simple pendulum model, [2]. 5
2.3 Pendulum model with planar liquid surface, [2]. 5
2.4 Schematic view of trammel pendulum, [4]. 6

3.1 Example of step-steer manoeuvre input, [7]. 10
3.2 Normalized roll angle at different liquid percentage, [7]. 10
3.3 Normalized roll angle at different steering angles, [7]. 11
3.4 Normalized roll angle at different vehicle's velocity, [7]. 12
3.5 Force exerted on tank during cornering, [2]. 13
3.6 Centre of gravity oscillation comparison with 20% filling height, [8]. 13
3.7 Centre of gravity oscillation comparison with 80% filling height, [8]. 14
3.8 Overturning with pendulum model, [8]. 15
3.9 Pendulum sloshing scheme. 20
3.10 Roll angles of different sloshing loads; - - 25% filled volume; ___ 50% filled volume; - . - . 75% filled volume; . . equivalent rigid cargo(50% filled), [12]. 24
3.11 Tractor's and trailer's roll angle with rigid load. 24
3.12 Tractor's and trailer's roll angle with sloshing load (50 %). 25
3.13 Tractor's and trailer's roll angle with sloshing load (75 %). 25
3.14 Roll angle comparison between analytical and SVT model, with rigid load (50 %). 26
3.15 Roll angle comparison between analytical and SVT model, with sloshing load (50 %). 27
3.16 Roll angle comparison between analytical and SVT model, with sloshing load (75 %). 27
3.17 Trailer's roll angles with different fluid levels percentage. 28
3.18 Normalized roll angle with different fluid levels percentage. 29
3.19 Lateral displacement of tractor and trailer with 50% load. 29

3.20 Single lane change driver's inputs. 30
3.21 Tractor's and trailer's roll angles during single lane change manoeuvre. 30
3.22 Trailer's roll angles during single lane change manoeuvre with different filling levels. 31
3.23 System's root locus when tank is filled at 50 % 32
3.24 System's root locus when tank is filled at 75 % 32
3.25 System's root locus when tank is filled at 50 % with a rigid load (detail view). 33
3.26 System's root locus when tank is filled at 50 % with a sloshing load (detail view). 33
3.27 Natural frequency and damping ratio of the system (50 % sloshing liquid). 34
3.28 Natural frequency and damping ratio of the system (75 % sloshing liquid). 34
3.29 System's bode plot when tank is filled at 50 % 35
3.30 System's bode plot when tank is filled at 75 % 35
3.31 Variation of natural frequency parameter of analytical model (a) and experimentally determined (b), [13]. 36

4.1 Normalized velocity of the semi-trailer at different load levels, [14]. . 38
4.2 Normalized pitch angle of the semi-trailer at different load levels, [14]. 39
4.3 Pitch angle and sprung mass vertical displacement in case of rigid load (solid black line), liquid unbaffled load (blue dotted line), liquid baffled load (red dotted line), [15]. 40
4.4 Longitudinal acceleration and velocity in case of rigid load (solid black line), liquid unbaffled load (blue dotted line), liquid baffled load (red dotted line), [15]. 41
4.5 Natural frequency parameter in function of liquid depth, [13]. . . . 42
4.6 Dimension of each element of cylindrical tank, [17]. 43
4.7 Longitudinal sloshing non-dimensional natural frequency in a horizontal cylinder. 44
4.8 Longitudinal acceleration in 40 % filled tank subjected to 0.3 g. . . . 46
4.9 Longitudinal acceleration in 60 % filled tank subjected to 0.3 g. . . . 46
4.10 Longitudinal acceleration in 40 % filled tank subjected to 0.3 g with impacts simulation. 48
4.11 Longitudinal acceleration in 60 % filled tank subjected to 0.3 g with impacts simulation. 48
4.12 Tires speed when tank is filled at 40 % while steering and braking. . 49
4.13 Yaw rate during steering and braking only with rear axle, [19]. . . . 50
4.14 Driver's input during jack-knife manoeuvre. 51

4.15 Yaw rate during steering and braking only with rear axle when tank is filled at 40 %. 51
4.16 Yaw rate during steering and braking only with rear axle when tank is filled at 60 %. 52
4.17 Yaw rate when braking only with rear axle when tank is filled at 40 %. 52
4.18 Yaw rate when braking only with rear axle when tank is filled at 50 %. 53
4.19 Yaw rate when braking only with rear axle when tank is filled at 70 %. 53
4.20 Tires speed when tank is filled at 40 % while braking. 54
4.21 Tires speed when tank is filled at 50 % while braking. 54
4.22 Tires speed when tank is filled at 70 % while braking. 55
4.23 Trailer pitch angle when tank is filled at 40 % while braking. 55
4.24 Trailer pitch angle when tank is filled at 50 % while braking. 56
4.25 Trailer pitch angle when tank is filled at 40 % while braking. 56
4.26 Vehicle's and trailer's yaw rate at different liquid filling levels. . . . 57
4.27 Tractor rear wheels speed at different liquid filling levels. 57
4.28 Trailer's pitch angle at different liquid filling levels. 58

B.1 Tractor scheme, [11]. 62
B.2 Trailer scheme., [11] 65

Chapter 1

Introduction

Tank vehicles are commonly used to transport and delivery liquid all around the world, but their freight can create critical problems related to road safety. In Italy in 2021, more than 18000 accidents (more than 6 %) were caused by heavy-duty vehicles [1] and among these, a considerable part can be related to the roll-over problem.

The roll-over affects all vehicles with high centre of gravity, and particularly those transporting liquids since they are subjected to the *sloshing* phenomenon. Sloshing is caused by an external force on a partially filled tank, for example, during a turn the vehicle is subjected to a centrifugal force which consequently induces transient force and moment on the trailer and on the vehicle itself. When the external excitation is at the same frequency of the natural one of the fluid, roll-over instability can happen. In order to analyse this problem different methods are used, such as numerical simulations. The main drawback of these numerical and CFD (Figure 1.1) analyses is the needing of long computational time, therefore in the past years different models have been developed in order to shorten it, keeping a good accuracy. The most used in literature are the equivalent mechanical systems since they are extremely cost effective and fast, achieving a good accuracy if properly calibrated. Examples of this type are the *mass-spring-damper model* and the *pendulum model*.

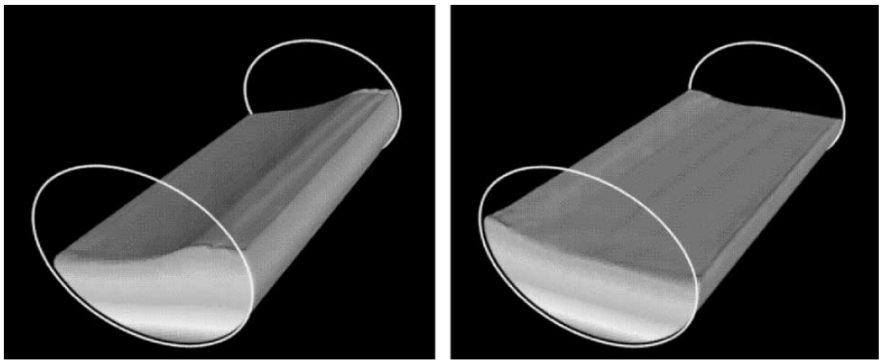

Figure 1.1: Example of lateral sloshing CFD simulation result, [2].

Chapter 2

Types of model

2.1 Equivalent mechanical models

2.1.1 Mass-spring-damper model

Mechanical models require the analysis of the so called *sloshing modes*. Anyway, modes greater than one usually are neglected in practical applications. This natural frequency is in the order of 0.6 Hz, which means that it coincides with most of the common frequency components during cornering manoeuvre.

To simplify the sloshing problem, mechanical models are based on several assumptions:

- the total mass, moment of inertia and centre of mass must be equal to those of original system;
- modes must be the same;
- liquid must exert the same impact on tank's walls.

For what concern the mass-spring-damper model, a fixed mass m_0 and several mobile masses m_n are present. The mobile masses are connected to the container through a spring k_n and a damper c_n, as depicted in Figure 2.1a. Moreover, the fluid is considered incompressible, irrotational and non-viscous, while capillarity and surface tensions have been neglected. With these considerations the following equation is obtained:

$$\ddot{x}_n + 2\zeta_n\omega_n\dot{x}_n + \omega_n^2 x_n = -\ddot{x}_0 \tag{2.1}$$

where ω_n is the natural frequency and ζ_n is the damping ratio. This formula can be used in the approximation of linear model, in order to have a almost planar free surface (Figure 2.1b). The model can become more complex including non-linearities, like non-planar liquid free surface, in order to analyse more complex sloshing motion, as Guagliumi et al. show in [3].

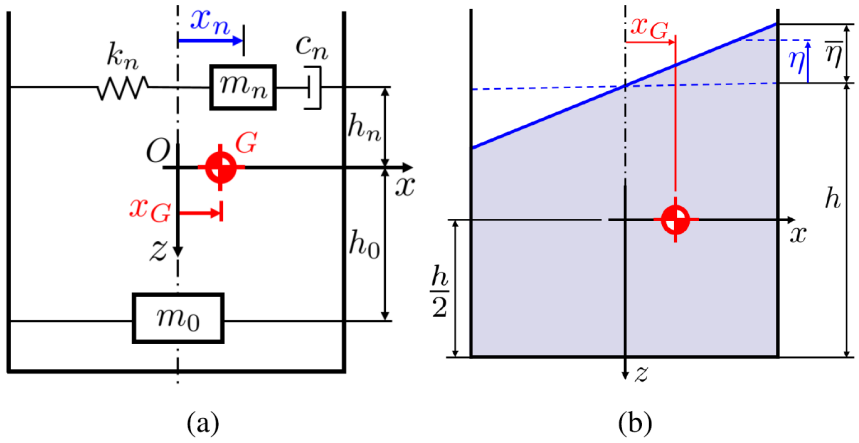

Figure 2.1: Mass-spring-damper model (a), free surface of the liquid (b), [3].

2.1.2 Simple pendulum model

In the pendulum model, the mass of the liquid is assumed to be concentrated in a point and attached to the arm R,as shown in Figure 2.2. Considering a circular shape for the tank, the equation of motion of the pendulum can be written:

$$\frac{d\dot{\theta}}{dt} = \frac{1}{R}(a\cos\theta - g\sin\theta) \tag{2.2}$$

where θ is the angle between the rod and vertical axis, $\dot{\theta}$ the angular speed and a and g are the horizontal and vertical accelerations. Integrating the equation 2.2 with null angle and speed as initial condition, it is possible to obtain the angular position at each desired time step:

$$\theta^{n+1} = \theta^n + \Delta t\omega^n + \frac{(\Delta t)^2}{4}\left[\frac{1}{R}(a\cos\theta^{n+1} - g\sin\theta^{n+1}) + \frac{1}{R}(a\cos\theta^n - g\sin\theta^n)\right] \tag{2.3}$$

where n represents the time step and Δt the time increment, [2].

The free surface of the liquid is assumed planar while the pendulum oscillates so that is always perpendicular to this plane. Taking as reference the Figure 2.3, if the direction of sloshing motion is x, the motion equation can be written as:

$$\ddot{\theta}_n + 2\zeta_n\omega_n\dot{\theta}_n + \omega_n^2\sin\theta_n = -\frac{\ddot{x}_0}{l_n}\cos\theta_n \tag{2.4}$$

and the sloshing height as:

$$\bar{\eta} = \frac{d}{2}\tan\theta_n \tag{2.5}$$

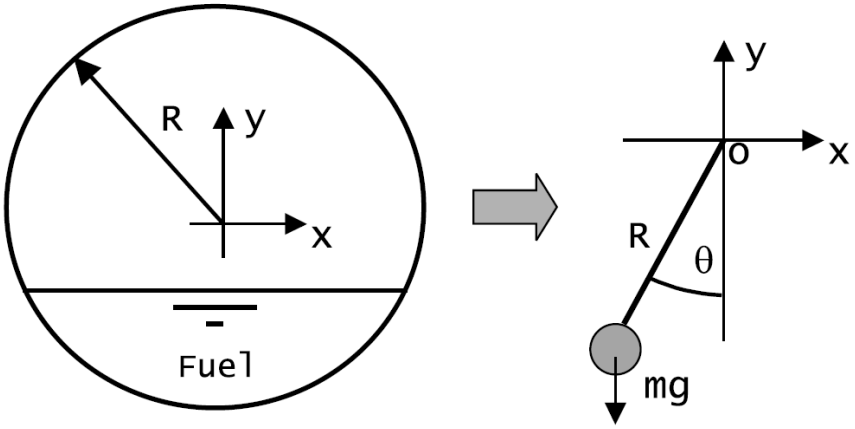

Figure 2.2: Scheme of simple pendulum model, [2].

where d is the tank diameter, ζ_n the damping ratio, ω_n the natural frequency and $l_n = R$ is the rod of pendulum. As shown in [3], linearising the equation 2.4 considering small angle, is possible to notice that $\bar{\eta}$ is not affected by the sloshing mass, meaning that is reasonable to take into account only the first-mode motion during sloshing. Sloshing height typically can vary between few millimetres and more than 60 mm, depending on the type of tank, type of motion, duration, acceleration and velocity.

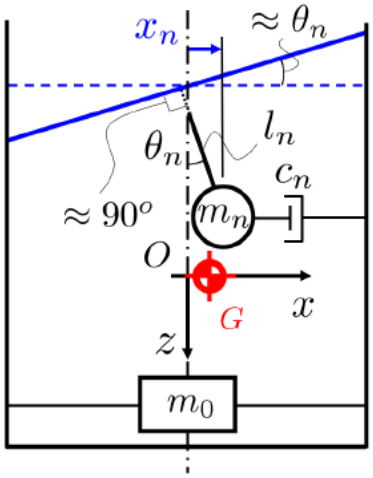

Figure 2.3: Pendulum model with planar liquid surface, [2].

2.1.3 Trammel pendulum model

Numerical simulations proved that what counts the most is the first-order sloshing mode and as result, the calculated centre of gravity trajectory of liquid is concentric to tank's periphery, both in case of circular and elliptical shape. Trammel pendulum is usually used, since it can describe the sloshing event with its elliptical swing. This kind of pendulum is made of two rods connected with each other with a

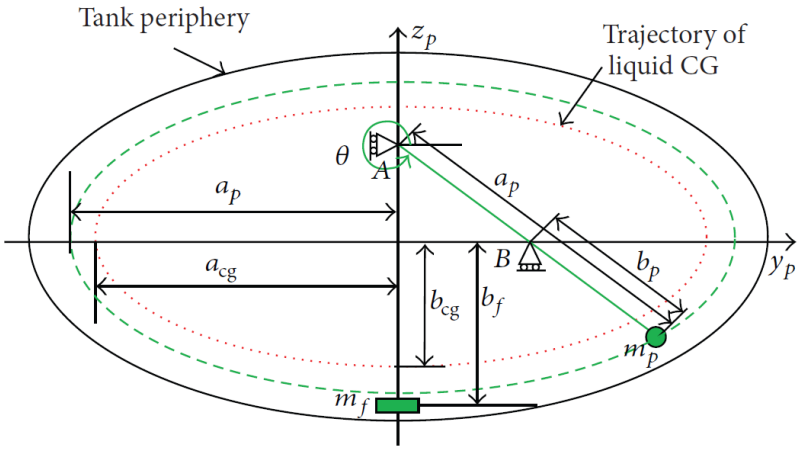

Figure 2.4: Schematic view of trammel pendulum, [4].

concentrated mass attached at its end, as can be seen in Figure 2.4. a_p and b_p are equal to half of major and minor axes of the pendulum trajectory respectively, a_{CG} and b_{CG} are half of the major and minor axes of the elliptical shape described by the motion of liquid bulk centre of mass, θ is the pendulum angular oscillation, m_p is the pendulum mass which represents the liquid sloshing and m_f is the fixed liquid mass. In fact, not all of the liquid inside the tank participates to sloshing event, therefore the use of a single mass would lead to wrong results. The motion equation with respect to the tank's inertia coordinate system fixed in its centre, can be written using the Lagrangian approach:

$$\ddot{\theta}(a_p^2 \sin^2\theta + b_p^2 \cos^2\theta) + \frac{1}{2}\dot{\theta}^2(a_p^2 - b_p^2)\sin 2\theta + g b_p \cos\theta = 0 \tag{2.6}$$

where b_p and m_p are function of the liquid fill level in the tank [4], while a_p can be obtained through the tank's width to height ratio λ:

$$\frac{a}{b} = \frac{a_{CG}}{b_{CG}} = \frac{a_p}{b_p} = \lambda; \qquad a_p = b_p \times \lambda \tag{2.7}$$

and the fixed mass is easily obtained from the total liquid bulk mass minus the pendulum one. Anyway, the tank cannot be considered a fixed reference frame since

it moves when the vehicle approaches a turn, or in general changes its direction. Therefore, new equations with respect to a non-inertial reference system must be derived. Usually the origin of this new system is located at the bottom of the tank and in this way the equation of motion can be written also in terms of roll angle.

As said before, only the first sloshing mode is considered and since the dynamic of trammel pendulum can be considered the same of the liquid sloshing, their oscillating frequency coincide and is approximately equal to 0.6 Hz. In reality this frequency should be obtained through numerical simulations, depending on the load, anyway a relation can be analytically written using the approximation of small oscillation angles:

$$\omega = \sqrt{\frac{g b_p}{a_p^2}} \tag{2.8}$$

Precision of pendulum models decreases as the height of liquid sloshing increases since the fluid has been approximated as a non-deformable body. Moreover, in this kind of models is quite difficult to determine a damping coefficient so it is usually neglected, even if in reality there is viscous friction in the liquid and at the tank boundary layer or some dissipation effect is present due to impact of fluid over the tank's walls. These last cases requires particular mathematical models which have been studied by Godderidge et al. in [5].

2.2 Fluid-solid coupling system

Other ways to analyse the sloshing phenomenon are the fluid-solid coupling systems, [6]. Multi-body systems based on estimation of liquid sloshing can be used, where the liquid bulk is simplified as a mass point so forces and torque can be easily obtained:

$$F_y = m g a_y; \qquad F_z = m g; \qquad M = \vec{r} \times \vec{F} \tag{2.9}$$

where F_y is the lateral sloshing force, F_z the vertical sloshing force, M the sloshing torque, $\vec{r}$ the position vector and $\vec{F}$ the force vector. Also the tilt angle of the liquid free surface can be calculated in first approximation, neglecting tank's shape and fill level:

$$\tan \theta_s = \frac{a_y + \varphi}{1 - a_y \varphi} \tag{2.10}$$

where a_y is the lateral acceleration and φ the tank's roll angle. For example, with a lateral acceleration of 0.1 g and a roll angle of $-1°$ the tilt angle is less than 1°. Increasing the roll angle is possible to observe an increment of θ_s as well, up to about 5°. In reality, when the lateral acceleration is greater than 0.1 g, the liquid free surface is not planar but curves and this changes also the location of the centre of mass position with respect to the linear case. Therefore, the computation of

forces can be obtained through the pressure exerted on the tank's wall with good results. As expected, from this analysis the sloshing is greatly influenced by lateral acceleration and liquid fill level, in particular between 40 % and 60 %. In fact, when the liquid level is greater than 60 % the sloshing part is smaller, so the vehicle roll stability is only slightly influenced by transient sloshing, as can be seen later in Figure 3.2.

In order to analyse the roll-over risk of tank vehicles a comparison with ordinary trucks can be done. Being φ_t the roll angle of a tank truck and φ_0 the roll angle of an ordinary one, it is possible to consider the *rate of decline*, defined has:

$$\text{rate of decline} = \left| \frac{\varphi_0 - \varphi_t}{\varphi_0} \right| \tag{2.11}$$

It is an adimensional quantity always bigger or equal to zero. The greater it is (usually no more than 1.8), the worst the behaviour of the partially liquid filled tank vehicles with respect to the ordinary trucks since sloshing greatly influence its stability. Simulation on different tank's shapes were performed showing that it has a great effect on roll, [6]. It has been observed that elliptical shaped tanks have better stability. One possible reason is that the vertical displacement of the bulk liquid centre of mass is lower in elliptical shape tanks than circular ones. It has been observed also that at certain point the increase of the major axis of the elliptical tank leads no more to improvements. This happens when the ratio between the major axis with the minor one reaches 1.5

Chapter 3

Lateral sloshing

3.1 Effects of different manoeuvres

Different standard manoeuvres can be used to analyse the sloshing phenomenon, either closed or open-loop. In order to understand the dynamic response of the vehicle in an objective way, it is common to use an open-loop approach so to not have any influence of the driver model. The *step-steer* is the most used one. A steering-wheel angle is applied as input, assuming that the driver is able to modify this angle almost instantaneously from zero to a certain value, as shown in Figure 3.1. In the case of interest, the output analysed is the roll angle.

Comparing tank vehicles and equivalent rigid cargo ones, the normalized roll angle of the semi-trailer can be introduced:

$$N\varphi_s = \frac{\varphi_s}{\varphi_{sr}} \tag{3.1}$$

where φ_s is the semi-trailer roll angle, while φ_{sr} the equivalent rigid cargo vehicle one. Tank vehicles have greater roll angle than rigid cargo ones, so $N\varphi_s \geq 1$ but usually lower than 2: the more it is far from unity, the more the deviation from ideality.

Mohammad Mahdi Jalili et al. [7], observed that increasing the steering angle, the amplitude of roll angle oscillations increases, due to an increased load transfer oscillation of the trailer caused by the sloshing fluid as shown in Figure 3.3. Similar conclusion can be drawn also analysing the same results but varying the speed of the vehicle (Figure 3.4). As expected, the bigger the speed, the greater the instability. This means that at low speed and low steering angle tank vehicles tends to behave as an equivalent rigid cargo vehicle, and vice versa increasing these parameters the stability is greatly influenced.

Another simple manoeuvre is the constant radius cornering. For example, in [2] a turn with radius equal to 250 m is run at the speed of 36 km/h. Looking

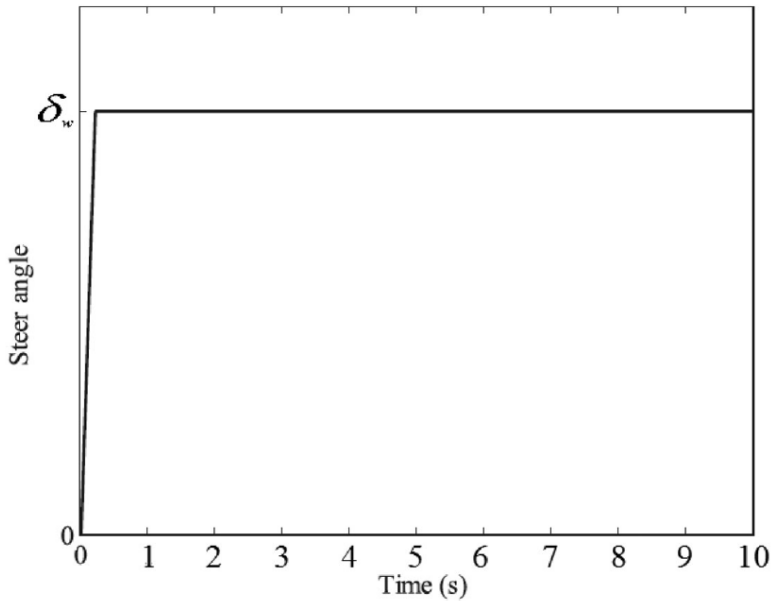

Figure 3.1: Example of step-steer manoeuvre input, [7].

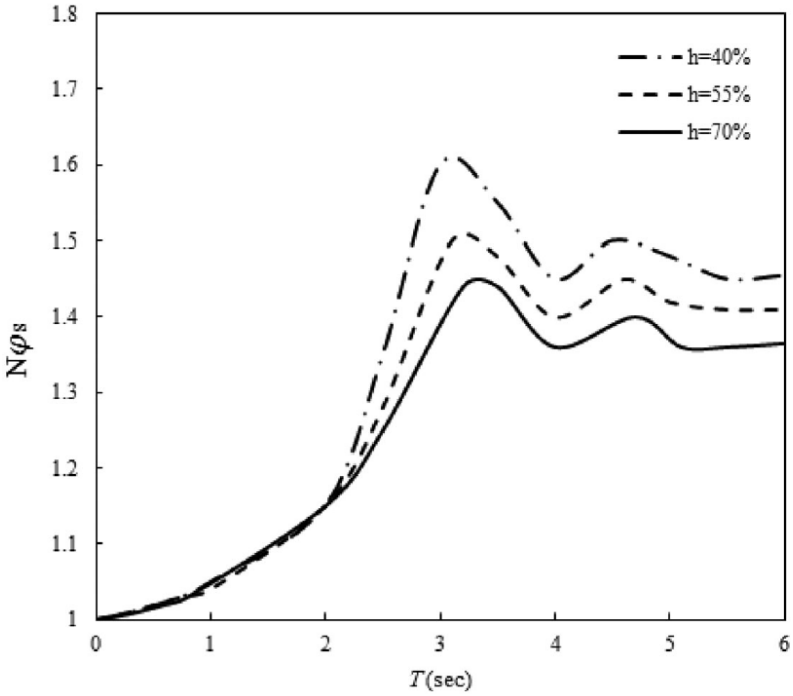

Figure 3.2: Normalized roll angle at different liquid percentage, [7].

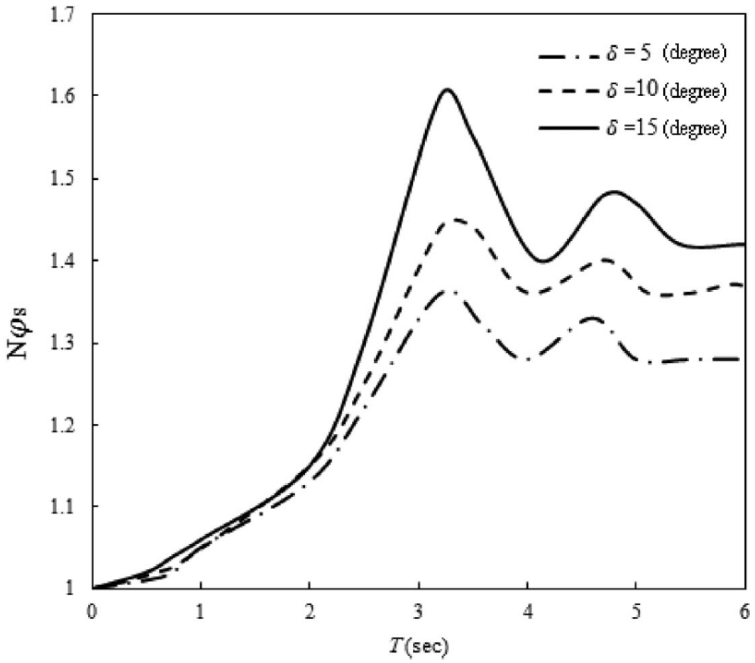

Figure 3.3: Normalized roll angle at different steering angles, [7].

at Figure 3.5, numerical simulation showed that the centrifugal force create an unstable displacement of the fluid contained in the tank.

More complex manoeuvre is the *double lane change*: starting from a rectilinear trajectory, the driver imposes a steering input in order to move in a parallel lane and then returns back to the original path. Comparing the results of a numerical model (Smooth Particle Hydrodynamics, [8]) and the pendulum one, is possible to observe in Figures 3.6 and 3.7 how both can properly represent the phenomenon and how the centre of gravity oscillates during this manoeuvre. The magnitude of the angle is quite high both in condition of partially-empty cargo and almost completely filled one, considering that in this case the imposed tangential velocity during cornering has been set to 40.25 km/h.

3.2 Overturning

It is clear that the sloshing can cause problems in stability, in particularly considering the overturning. This instability is due to the motion of the liquid centre of gravity inside the tank. To understand properly this problem is necessary to analyse the liquid lateral motion. For this kind of analysis a steady-turning manoeuvre and some assumptions are taken into account:

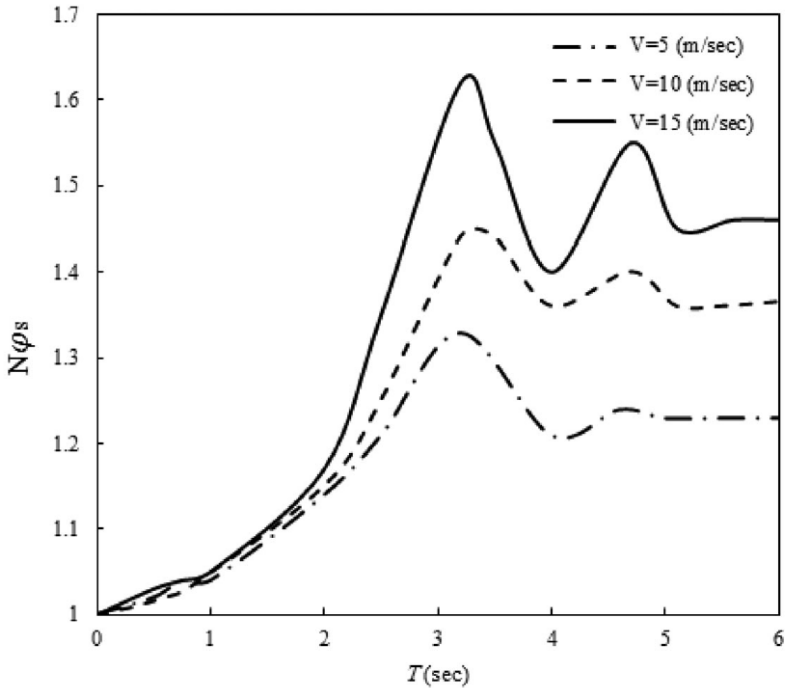

Figure 3.4: Normalized roll angle at different vehicle's velocity, [7].

- small roll angle;
- linear roll stiffness and damping;
- yaw, longitudinal and vertical motions have been neglected;
- ideal fluid (negligible viscosity, incompressible and irrotational flow);
- rigid container;
- negligible roll motion of lumped unsprung mass.

Based on these assumptions, it is possible to estimate the roll-over lateral acceleration threshold, which is the maximum acceleration sustained by the vehicle before the tires in the inner side of the turn start to lift off.

The estimation for roll-over threshold can be computed from the analysis of the simple pendulum model. In particular, as depicted in equation 2.2, the pendulum acceleration is:

$$a_y = a\cos\theta - g\sin\theta \tag{3.2}$$

so the force in the rod can be expressed as:

$$F_v = m_L a_y \tag{3.3}$$

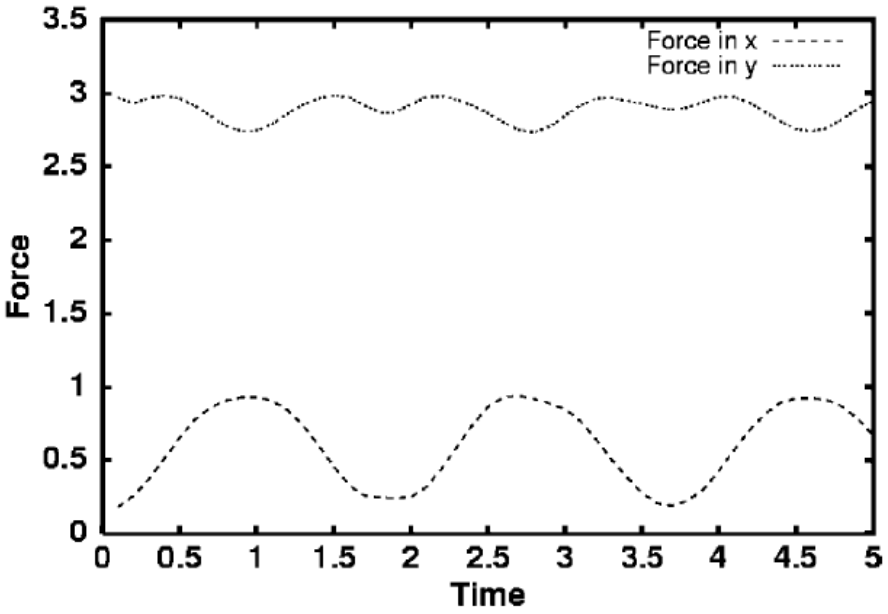

Figure 3.5: Force exerted on tank during cornering, [2].

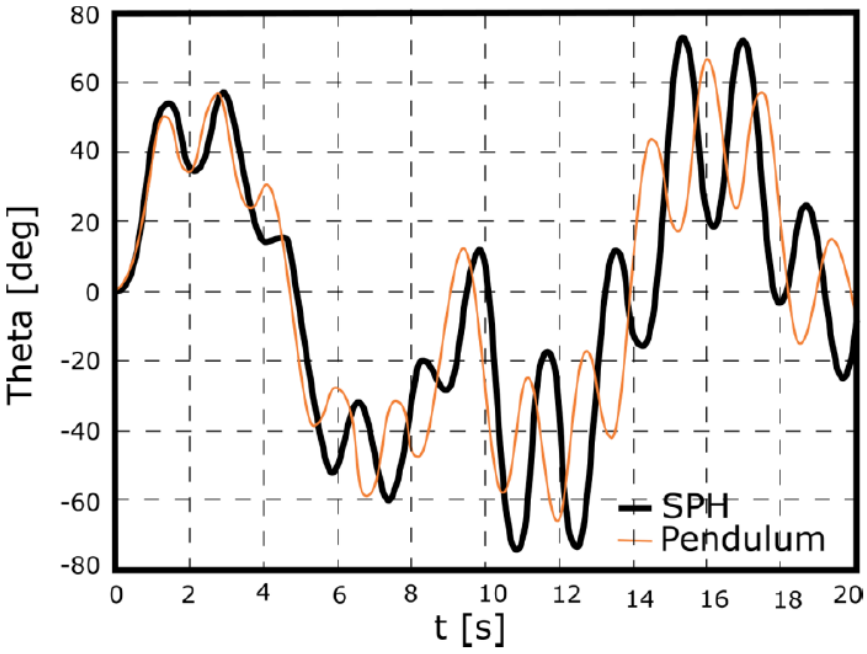

Figure 3.6: Centre of gravity oscillation comparison with 20% filling height, [8].

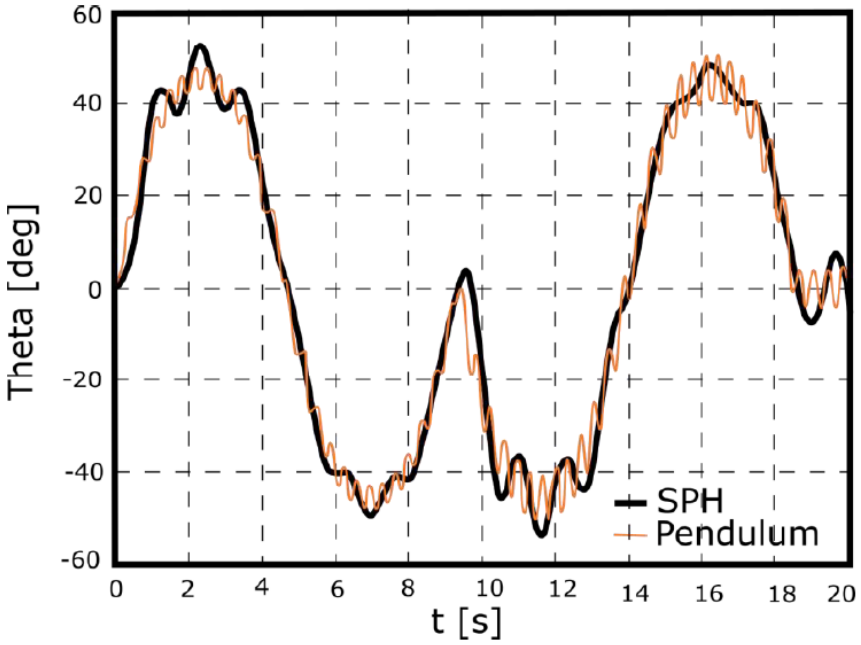

Figure 3.7: Centre of gravity oscillation comparison with 80% filling height, [8].

where m_L is the mass of the sloshing liquid. The overturning moment can be expressed as the sum of two contributions: vehicle and oscillating liquid moment. The vehicle moment contribution can be written as:

$$M_T = -m_T a_y h_T \tag{3.4}$$

where m_T is the vehicle's mass and h_T the distance between the ground and the roll centre. Analogous analysis can be done for the liquid contribution:

$$M_L = F_c h_s \sin\theta \tag{3.5}$$

where F_c is the force of the liquid in the tank which is equal to the rod force F_v (calculated in equation 3.3) with opposite sign, while h_s is the distance between ground and centre of the tank, as shown in Figure 3.8.

When the overturning moment overcome the restoring moment, there is roll-over. Restoring moment depends on the position of the centre of gravity of the sloshing liquid, which can be determined through the pendulum's inclination. Since small angles have been assumed and referring to Figure 3.8, restoring moment can be written as:

$$M_R = (m_T + m_L)gt \tag{3.6}$$

where m_T is the vehicle's mass, m_L the liquid one and t is the vehicle's half width.

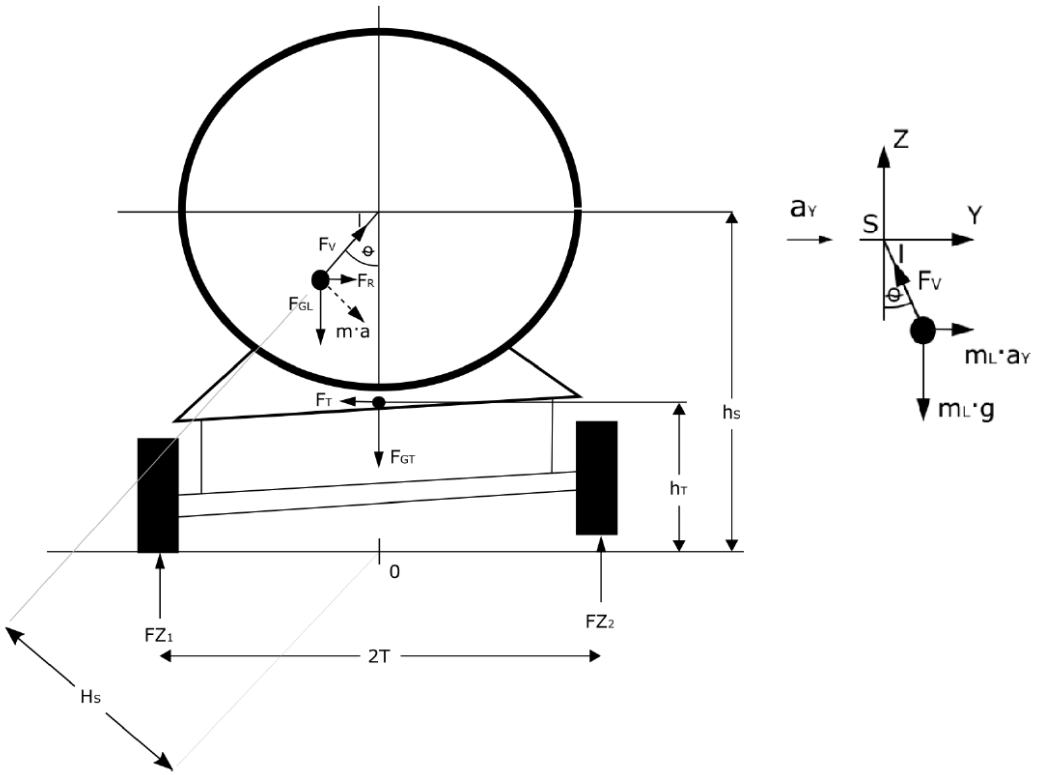

Figure 3.8: Overturning with pendulum model, [8].

A simple way to characterize the roll-over event can be the *overturning risk factor* R, defined in [10]. It uses the wheel load to determine when this event starts. It is defined as:

$$R = \left|1 - \frac{P_d}{P_s}\right| \tag{3.7}$$

where P_d is the dynamic load of the outer side wheel, while P_s is the static load. R can take all the values between 0 and 1, and when it reaches the unity the overturning starts. For example, when the tank is filled at 50 % with an harmonic oscillation frequency between 0.5 Hz and 0.6 Hz, R reaches 1 easily with a lateral acceleration greater than $2\,\mathrm{m/s^2}$. The static load when the vehicle is not turning is equal on both wheels:

$$P_s = \frac{(m + m_l)g - F_{zd}}{2} \tag{3.8}$$

where F_{zd} is the vertical dynamic liquid force and m_l is the load mass. Instead, the dynamic load depends on the kind of model.

3.3 Analytical lateral model

The model presented in this section is a linear system taken from [11]. It is useful to easily represent the handling and roll dynamic of a heavy-duty vehicle. In this model the equations related to pitch and heave are not included since they have only a small influence on roll behaviour. Moreover, also aerodynamic and road disturbances are neglected and, in order to linearize the model, all the angles are assumed to be small.

All vehicle's parameters name and data are summed up in Appendix A and B, taken from the references [12] and [11].

3.3.1 Rigid vehicle model

Each vehicle unit is made by a single body which represents the sprung mass. The tractor is free to side-slip, yaw and roll, while the trailer can yaw and roll. The systems has a total of 5 degree of freedom.

The tractor is a two axle vehicle unit. In particular it has a pair of single tires mounted on the front axle, and a pair of twin tires at the rear axle. Instead the trailer shows three axles with pairs of single tires.

To simplify the simulation, in this particular case, the tank has a circular cross-section and the forward speed is kept constant, so there will be no longitudinal acceleration.

The equations of the tractor are:

$$-I'_{1xz}\ddot{\varphi}_1 + I'_{1zz}\ddot{\psi}_1 = N_{\beta_1}\beta_1 + N_{\dot{\psi}_1}\dot{\psi}_1 + N_\delta\delta - b'_{f1}F_{cy} \tag{3.9}$$

$$\begin{aligned} I'_{1xx}\ddot{\varphi}_1 - I_{1xz}\ddot{\psi}_1 = {} & m_{s1}gh_{s1}\varphi_1 - m_{s1}Uh_{s1}(\dot{\beta}_1 + \dot{\psi}_1) + \\ & - (k_{f1} + k_{r1})\varphi_1 - (L_{f1} + L_{r1})\dot{\varphi}_1 - k_\varphi(\varphi_1 - \varphi_2) + (r_1 - h_{ar1})F_{cy} \end{aligned} \tag{3.10}$$

The lateral force F_{cy} exchanged between tractor and trailer in the articulation point is a dependent variable and can be expressed in function of the independent ones:

$$F_{cy} = -m_{s1}h_{s1}\varphi_1 - m_1U(\dot{\beta}_1 + \dot{\psi}_1) + Y_{\beta_1}\beta_1 + Y_{\dot{\psi}_1}\dot{\psi}_1 + Y_\delta\delta \tag{3.11}$$

The kinematic constraint between tractor and trailer is expressed through the following equation:

$$\dot{\beta}_1 - \dot{\beta}_2 - \frac{r_1 - h_{ar1}}{U}\ddot{\varphi}_1 + \frac{r_2 - h_{af2}}{U}\ddot{\varphi}_2 + \frac{b'_{r1}}{U}\ddot{\psi}_1 - \frac{b'_{f2}}{U}\ddot{\psi}_2 + \dot{\psi}_1 - \dot{\psi}_2 = 0 \tag{3.12}$$

For what concerns the trailer, there are three more equations:

$$-I'_{2xz}\ddot{\varphi}_2 + I'_{2zz}\ddot{\psi}_2 = N_{\beta_2}\beta_2 + N_{\dot{\psi}_2}\dot{\psi}_2 + b'_{f2}F_{cy} \tag{3.13}$$

$$I'_{2xx}\ddot{\varphi}_2 - I_{2xz}\ddot{\psi}_2 = m_{s2}gh_{s2}\phi_2 - m_{s2}Uh_{s2}(\dot{\beta}_2 + \dot{\psi}_2) + \\ - k_2\varphi_2 - L2\dot{\varphi}_2 + k_\phi(\varphi_1 - \varphi_2) - (r_2 - h_{af2})F_{cy} \quad (3.14)$$

$$m_{s2}h_{s2}\ddot{\varphi}_2 = -m_2U(\dot{\beta}_2 + \dot{\psi}_2) + Y_{\beta_2}\beta_2 + Y_{\dot{\psi}_2}\dot{\psi}_2 + F_{cy} \quad (3.15)$$

Roll motion of axles is neglected and the equivalent roll stiffness due to tire and suspensions is given by:

$$\frac{1}{K_{i,eq}} = \frac{1}{k_{susp,i}} + \frac{1}{k_{tire,i}} \quad (3.16)$$

where i is the generic axle.

This set of equations can be written in state-space representation:

$$\dot{x} = Ax + B\delta \quad (3.17)$$

where:

$$x = \begin{bmatrix} \beta_1 & \dot{\psi}_1 & \varphi_1 & \dot{\varphi}_1 & \beta_2 & \dot{\psi}_2 & \varphi_2 & \dot{\varphi}_2 \end{bmatrix}^\top \quad (3.18)$$

$$E = \begin{bmatrix} -m_1Ub'_{f1} & I'_{1zz} & 0 & -I'_{1xz} - m_{s1}h_{s1}b'_{f1} \\ m_{s1}Uh_1 + (r_1 - h_{ar1})m_1U & -I'_{1xz} & 0 & I'_{1xx} + m_{s1}h_1(r_1 - h_{ar1}) \\ 0 & 0 & 1 & 0 \\ 1 & \frac{b'_{f1}}{U} & 0 & \frac{-(r_1 - h_{ar1})}{U} \\ b'_{f2}m_1U & 0 & 0 & b'_{f2}m_{s1}h_1 \\ -(r_2 - h_{af2})m_1U & 0 & 0 & -(r_2 - h_{af2})m_{s1}h_1 \\ m_1U & 0 & 0 & m_{s1}h_1 \\ 0 & 0 & 0 & 0 \end{bmatrix} \\ \begin{bmatrix} 0 & 0 & 0 & 0 \\ 0 & 0 & 0 & 0 \\ 0 & 0 & 0 & 0 \\ -1 & \frac{-b'_{f2}}{U} & 0 & \frac{(r_2 - h_{af2})}{U} \\ 0 & I'_{2zz} & 0 & -I'_{2xz} \\ m_{s2}Uh_2 & -I'_{2xz} & 0 & I'_{2xx} \\ m_2U & 0 & 0 & m_{s2}h_2 \\ 0 & 0 & 1 & 0 \end{bmatrix} \quad (3.19)$$

$$A = E^{-1}\begin{bmatrix} A_1 & A_2 & A_3 \end{bmatrix} \quad (3.20)$$

$$A_1 = \begin{bmatrix} N_{\beta_1} - b'_{f1}Y_{\beta_1} & b'_{f1}(m_1U - Y_{\psi_1}) + N_{\psi_1} \\ Y_{\beta_1}(r_1 - h_{ar1}) & -m_{s1}Uh_1 + (r_1 - h_{ar1})(Y_{\psi_1} - m_1U) \\ 0 & 0 \\ 0 & -1 \\ b'_{f2}Y_{\beta_1} & b'_{f2}(-m_1U + Y_{\dot{\psi}_1}) \\ -(r_2 - h_{af2})Y_{\beta_1} & -(r_2 - h_{af2})(Y_{\dot{\psi}_1} - m_1U) \\ Y_{\beta_1} & Y_{\dot{\psi}_1} - m_1U \\ 0 & 0 \end{bmatrix} \tag{3.21}$$

$$A_2 = \begin{bmatrix} 0 & 0 & 0 \\ -k_\phi - (K_{1f,eq} + K_{1r,eq}) + m_{s1}gh_1 & -(L_{1f} + L_{1r}) & 0 \\ 0 & 1 & 0 \\ 0 & 0 & 0 \\ 0 & 0 & N_{\beta_2} \\ k_\phi & 0 & 0 \\ 0 & 0 & Y_{\beta_2} \\ 0 & 0 & 0 \end{bmatrix} \tag{3.22}$$

$$A_3 = \begin{bmatrix} 0 & 0 & 0 \\ 0 & k_\varphi & 0 \\ 0 & 0 & 0 \\ 1 & 0 & 0 \\ N_{\dot{\psi}_2} & 0 & 0 \\ -m_{s2}Uh_2 & m_{s2}gh_2 - K_{2,eq} - k_\varphi & -L_2 \\ -m_2U + Y_{\dot{\psi}_2} & 0 & 0 \\ 0 & 0 & 1 \end{bmatrix} \tag{3.23}$$

$$B = E^{-1} \begin{bmatrix} -b'_{f1}Y_\delta + N_\delta \\ (r_1 - h_{ar1})Y_\delta \\ 0 \\ 0 \\ b'_{f2}Y_\delta \\ -(r_2 - h_{af2})Y_\delta \\ Y_\delta \\ 0 \end{bmatrix} \tag{3.24}$$

with h_1 and h_2 representing the vertical distances between sprung mass centre of gravity and roll axis. All the derivatives of stability introduced with the letters Y and N are so defined:

$$Y_\beta = -C_f - C_r; \qquad Y_{\dot{\psi}} = -\frac{aC_f - bC_r}{U}; \qquad Y_\delta = C_f; \tag{3.25}$$

$$N_\beta = -(aC_f - bC_r); \qquad N_{\dot{\psi}} = -\frac{a^2C_f + b^2C_r}{U}; \qquad N_\delta = aC_f \tag{3.26}$$

where a and b represent the distance between front axle to total centre of mass, and from rear axle to total centre of mass, while C_i represents the cornering stiffness of the whole axle. Considering the non-linear behaviour of tires, it is possible to write a quadratic equation to describe the cornering stiffness:

$$C_i = c_1 F_z + c_2 F_z^2 \tag{3.27}$$

where F_z is the tire vertical load.

3.3.2 Simple pendulum sloshing model

The sloshing mass in the tank is simplified as a point mass free to oscillate around the vehicle tank's longitudinal axis through a rod. The law governing the pendulum's dynamic is given by the equation:

$$\ddot{\theta} + 2\zeta\omega\dot{\theta} + \omega^2\theta = \frac{a_y}{l} \tag{3.28}$$

where θ is the angle described by the pendulum's oscillations, ζ is the damping ratio due to liquid viscosity, ω is the system's natural frequency, l is the pendulum's rod length. In a simplified model where the steering angle is small, the lateral acceleration can be written as:

$$a_y = -\frac{U^2}{a_{r1}^*}\delta \tag{3.29}$$

Anyway, the mass involved in sloshing is not the entire liquid mass. For this reason, tanking into account the results showed in [6], it is possible to define a sloshing mass (represented by the pendulum) and a fixed one:

$$\begin{aligned} C_M = 0.7844 - 1.7290\Delta + 0.3351\lambda + 1.1560\Delta^2 + 0.7256\lambda\Delta + \\ - 0.1254\lambda^2 - 0.3219\Delta^3 - 0.9152\lambda\Delta^2 + 0.08043\lambda^2\Delta \end{aligned} \tag{3.30}$$

$$m_{pend} = m_{liq} C_M \tag{3.31}$$

$$m_{fix} = m_{liq} - m_{pend} \tag{3.32}$$

where Δ is the liquid fill percentage measured as the ratio between the liquid level height and the tank diameter, and λ is the ratio between tank's width to its length, which in this case is equal to 1 since the tank has circular section.

The same can be said for the oscillating mass' centre of gravity. In this case the pendulum's rod is defined as:

$$\begin{aligned} l = R(1.087 + 0.6999\Delta - 0.1407\lambda - 0.9291\Delta^2 - 1.178\lambda\Delta + \\ + 0.05495\lambda^2 - 0.03353\Delta^3 + 0.5404\lambda\Delta^2 + 0.1518\lambda^2\Delta) \end{aligned} \tag{3.33}$$

For what concerns the natural frequency and the damping ratio, they can be calculated based what written in [13]:

$$\omega = \sqrt{\frac{g}{l}} \tag{3.34}$$

$$\zeta = 0.131 \left(\frac{K}{0.08347}\right)^{0.718} \tag{3.35}$$

where K is a constant which depends on the liquid filling level:

$$K = \begin{cases} 0.08347 C_B^{0.5} \frac{1+0.46\left(2-\frac{h}{R}\right)}{1.46\left(2-\frac{h}{R}\right)} & h \geq R \\ 0.08347 C_B^{0.5} \frac{R}{h} & 0.1R \leq h \leq R \\ C_{10\%}(4.98\nu^{0.5} R^{-3/4} g^{-1/4}) & h < 0.1R \end{cases} \tag{3.36}$$

and where $C_{10\%}$ is a constant usually greater than 8 for liquid level below 10 %, while C_B is so defined:

$$C_B = \frac{10^4}{2\sqrt{2}} \nu R^{-3/2} g^{-1/2} \tag{3.37}$$

These are just empirical formulas that allows to linearize the sloshing motion, however, it is usually a non-linear problem and for this reason, in some cases, it needs to be analysed with different methods.

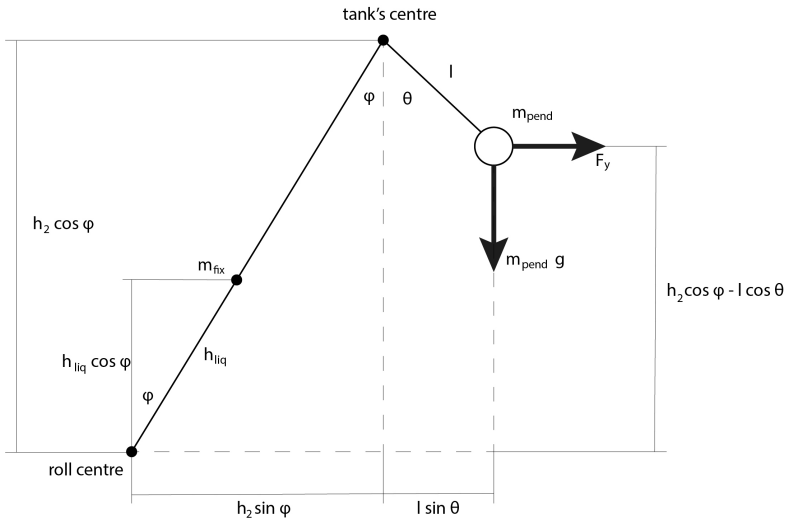

Figure 3.9: Pendulum sloshing scheme.

Looking at Figure 3.9, now it is possible to write the force and moment which cause a change in the vehicle's roll dynamic. The lateral force depends on the

oscillating mass and on acceleration as previously defined:

$$F_{y,pend} = m_{pend} a_y \tag{3.38}$$

while, taking into consideration the small angles assumption, the moment around the trailer's roll axis is:

$$M_{x,pend} = F_{y,pend}(h_2 - l) + m_{pend} g h_2 \varphi + l\theta \tag{3.39}$$

where h_2 is the distance between geometrical centre of tank and roll axis,φ is the trailer's roll angle. Also the fixed mass contributes to roll motion, through:

$$M_{x,fix} = F_{y,fix}(h_2 - h_{fix}) + m_{fix} g h_{fix} \varphi \tag{3.40}$$

where h_{fix} is the distance between fixed mass centre of mass and trailer's roll axis.

It is possible then to rewrite the vehicle's equations including the pendulum's dynamic:

$$x = \begin{bmatrix} \beta_1 & \dot{\psi}_1 & \varphi_1 & \dot{\varphi}_1 & \beta_2 & \dot{\psi}_2 & \varphi_2 & \dot{\varphi}_2 & \dot{\theta} & \theta \end{bmatrix}^\top \tag{3.41}$$

$$E = \begin{bmatrix} -m_1 U b'_{f1} & I'_{1zz} & 0 & -I'_{1xz} - m_{s1} h_{s1} b'_{f1} \\ m_{s1} U h_1 + (r_1 - h_{ar1}) m_1 U & -I'_{1xz} & 0 & I'_{1xx} + m_{s1} h_1 (r_1 - h_{ar1}) \\ 0 & 0 & 1 & 0 \\ 1 & \frac{b'_{f1}}{U} & 0 & \frac{-(r_1 - h_{ar1})}{U} \\ b'_{f2} m_1 U & 0 & 0 & b'_{f2} m_{s1} h_1 \\ -(r_2 - h_{af2}) m_1 U & 0 & 0 & -(r_2 - h_{af2}) m_{s1} h_1 \\ m_1 U & 0 & 0 & m_{s1} h_1 \\ 0 & 0 & 0 & 0 \\ 0 & 0 & 0 & 0 \\ 0 & 0 & 0 & 0 \end{bmatrix}$$

$$\begin{bmatrix} 0 & 0 & 0 & 0 & 0 & 0 \\ 0 & 0 & 0 & 0 & 0 & 0 \\ 0 & 0 & 0 & 0 & 0 & 0 \\ -1 & \frac{-b'_{f2}}{U} & 0 & \frac{(r_2 - h_{af2})}{U} & 0 & 0 \\ 0 & I'_{2zz} & 0 & -I'_{2xz} & 0 & 0 \\ m_{s2} U h_2 & -I'_{2xz} & 0 & I'_{2xx} & 0 & 0 \\ m_2 U & 0 & 0 & m_{s2} h_2 & 0 & 0 \\ 0 & 0 & 1 & 0 & 0 & 0 \\ 0 & 0 & 0 & 0 & 1 & 0 \\ 0 & 0 & 0 & 0 & 0 & 1 \end{bmatrix} \tag{3.42}$$

$$A = E^{-1}\begin{bmatrix} A_1 & A_2 & A_3 & A_4 \end{bmatrix} \tag{3.43}$$

$$A_1 = \begin{bmatrix} N_{\beta_1} - b'_{f1}Y_{\beta_1} & b'_{f1}(m_1U - Y_{\psi_1}) + N_{\psi_1} \\ Y_{\beta_1}(r_1 - h_{ar1}) & -m_{s1}Uh_1 + (r_1 - h_{ar1})(Y_{\psi_1} - m_1U) \\ 0 & 0 \\ 0 & -1 \\ b'_{f2}Y_{\beta_1} & b'_{f2}(-m_1U + Y_{\dot{\psi}_1}) \\ -(r_2 - h_{af2})Y_{\beta_1} & -(r_2 - h_{af2})(Y_{\dot{\psi}_1} - m_1U) \\ Y_{\beta_1} & Y_{\dot{\psi}_1} - m_1U \\ 0 & 0 \\ 0 & 0 \\ 0 & 0 \end{bmatrix} \tag{3.44}$$

$$A_2 = \begin{bmatrix} 0 & 0 & 0 \\ -k_\phi - (K_{1f,eq} + K_{1r,eq}) + m_{s1}gh_1 & -(L_{1f} + L_{1r}) & 0 \\ 0 & 1 & 0 \\ 0 & 0 & 0 \\ 0 & 0 & N_{\beta_2} \\ k_\phi & 0 & 0 \\ 0 & 0 & Y_{\beta_2} \\ 0 & 0 & 0 \\ 0 & 0 & 0 \\ 0 & 0 & 0 \end{bmatrix} \tag{3.45}$$

$$A_3 = \begin{bmatrix} 0 & 0 & 0 \\ 0 & k_\varphi & 0 \\ 0 & 0 & 0 \\ 1 & 0 & 0 \\ N_{\dot{\psi}_2} & 0 & 0 \\ -m_{s2}Uh_2 & m_{s2}gh_2 - K_{2,eq} - k_\varphi + m_{fix}gh_{fix} + m_{pend}gh_2 & -L_2 \\ -m_2U + Y_{\dot{\psi}_2} & 0 & 0 \\ 0 & 0 & 1 \\ 0 & 0 & 0 \\ 0 & 0 & 0 \end{bmatrix} \tag{3.46}$$

$$A_4 = \begin{bmatrix} 0 & 0 \\ 0 & 0 \\ 0 & 0 \\ 0 & 0 \\ 0 & 0 \\ 0 & m_{pend}gl \\ 0 & 0 \\ 0 & 0 \\ -2\zeta\omega & -\omega^2 \\ 1 & 0 \end{bmatrix} \tag{3.47}$$

$$B = E^{-1} \begin{bmatrix} -b'_{f1}Y_\delta + N_\delta \\ (r_1 - h_{ar1})Y_\delta \\ 0 \\ 0 \\ b'_{f2}Y_\delta \\ -(r_2 - h_{af2})Y_\delta + m_{liq}a_y(h_2 - h_{liq}) \\ Y_\delta + m_{liq}a_y \\ 0 \\ a_y/l \\ 0 \end{bmatrix} \tag{3.48}$$

In this brief analysis the pendulum's moment around z axis (M_z) is equal to zero since longitudinal sloshing has been neglected.

3.3.3 Analytical model results

With the analytical model shown previously is possible to analyse a step-steer manoeuvre easily. In the case of interest, the vehicle moves with a longitudinal speed of 60 km/h and starts to steer by 2° after 1 s.

As can be noticed in Figure 3.11, tractor's and trailer's roll angles reach quite soon the steady-state value, since the load has been considered rigid in that case. Moreover, comparing the results with the reference [12] (Figure 3.10), it can be seen the the steady-state values are both around 0.03 rad.

Considering instead the movement of the liquid, the roll response of the vehicle changes. Roll angles at steady-state increases with the liquid level since the mass of the load increases. An interesting observation can be done looking at the oscillations: in Figure 3.12 where the 50 % case is analysed, the liquid sloshing is more prevalent than the 75 % one (Figure 3.13). This is caused by the amount of mass that can actually oscillate. In fact, as said previously, part of the mass do not participate in the sloshing motion. Increasing the liquid level does not necessary mean that more

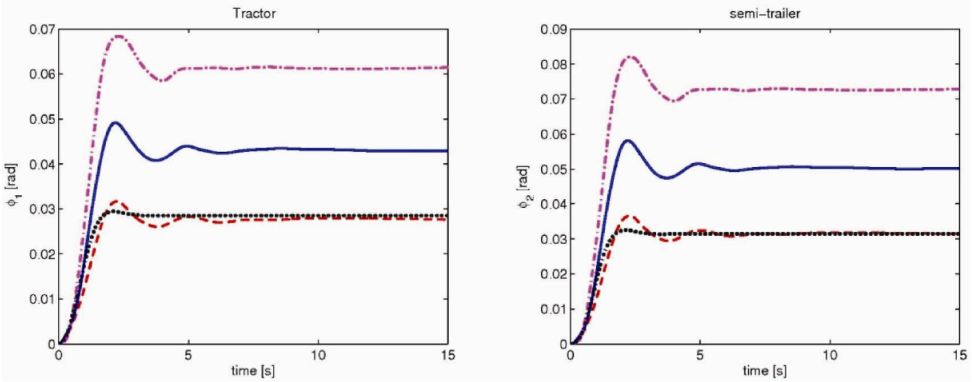

Figure 3.10: Roll angles of different sloshing loads; - - 25% filled volume; ___ 50% filled volume; - . - . 75% filled volume; . . equivalent rigid cargo(50% filled), [12].

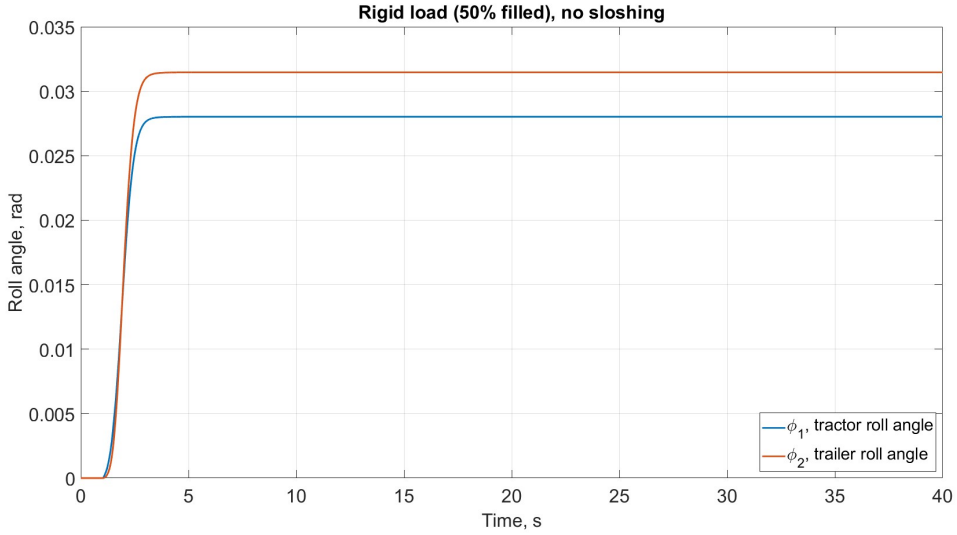

Figure 3.11: Tractor's and trailer's roll angle with rigid load.

mass in sloshing. Comparing these results with the reference Figure 3.10, it can be seen that the pendulum model is quite accurate and it can be used to represent the sloshing event in case of low steer angles and low lateral accelerations.

3.3.4 *Simscape Vehicle Template* simulations

Through the package *Simscape Vehicle Templates* has been possible to simulate a step steer manoeuvre in Matlab environment. This package developed by Steve Miller allows also to simulate the sloshing phenomenon using a general truck and trailer. First of all, vehicle mass, inertia, geometry, stiffness and damping have

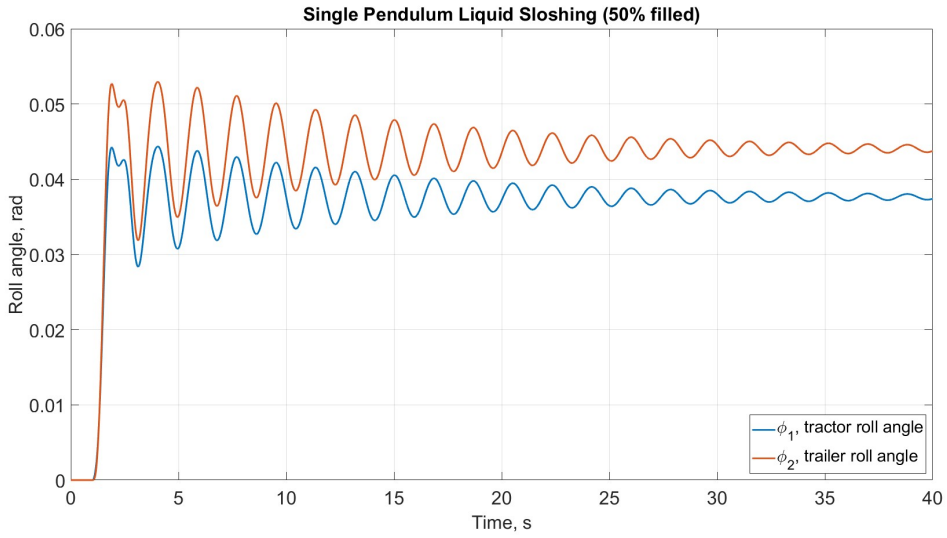

Figure 3.12: Tractor's and trailer's roll angle with sloshing load (50 %).

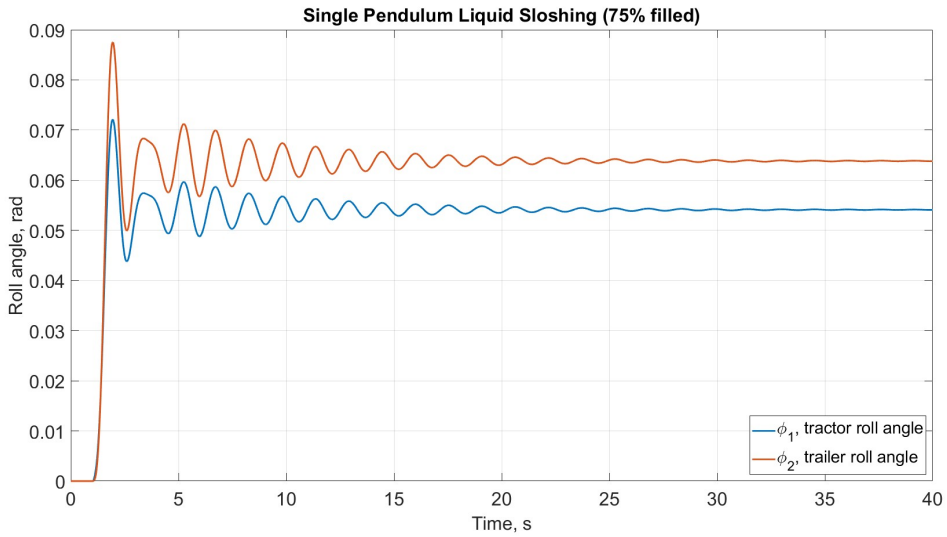

Figure 3.13: Tractor's and trailer's roll angle with sloshing load (75 %).

been updated as in [12] and [11]. Moreover, also the number of axles have been modified. In particular, the trailer shows now one more axle with respect to the default one, to a total of 3. For what concerns the tractor, it has been decided to not remove the third axle but to merge the two rear axles into a single one. This is has been achieved by neglecting one suspension system and modifying tires stiffnesses accordingly, in order to create an equivalent single rear axle, as depicted

in the reference article. In this section the *Simscape Vehicle Template* model has been compared to the analytical model described in chapter 3.3.2.

The fluid in case of rigid load is approximated as a solid block which is locked, so it is fixed to trailer's body. The amount of mass can be easily modified changing the liquid height to fill ratio.

In case of pendulum sloshing, SVT model assumes that all the liquid mass is sloshing. In order to take into account the considerations done in chapter 3.3.2, the fixed mass must be divided by the oscillating mass. For what concerns the pendulum, the rod length and pendulum's mass is calculated through the equations 3.31 and 3.33. The fixed mass is approximated as a solid which is fixed to tank and so it is not free to move.

In this case, the manoeuvre is a step-steer one, where the vehicle is running at 60 km/h and stats to steer at 0 s with a steering angle at wheels of 2°.

As can be seen in Figures 3.14, 3.15 and 3.16, SVT and analytical models show similar results, not too far from the reference one (Figure 3.10), especially at steady-state. Apart in the first transient phase, the roll angle of both tractor and trailer reach the expected values. Anyway, the pendulum's method sometimes can results not precisely correct. In fact, the sloshing event is almost never a linear problem and in presence of high lateral acceleration and high steering angle these models can give incorrect results.

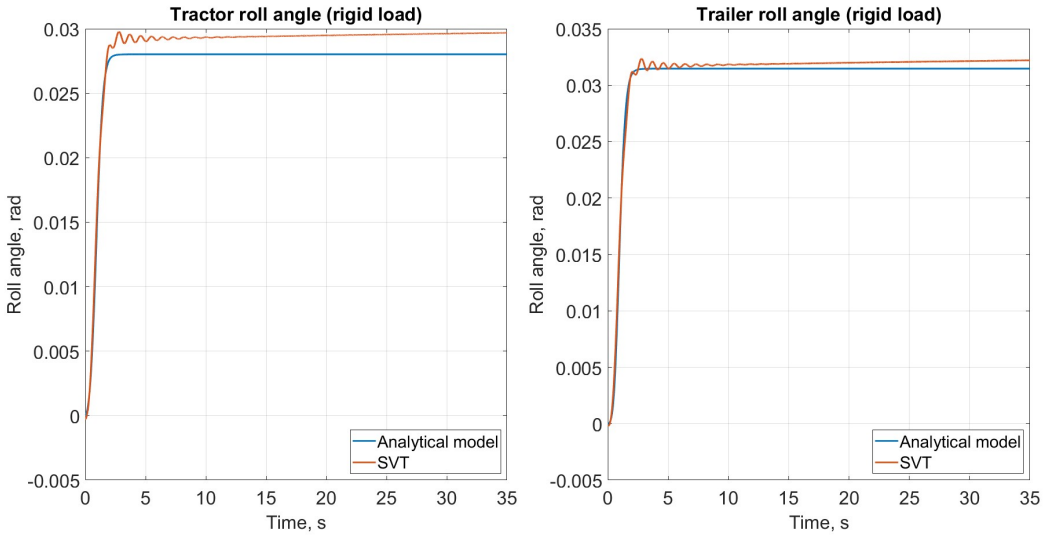

Figure 3.14: Roll angle comparison between analytical and SVT model, with rigid load (50 %).

In order to compare roll dynamic with different liquid level, Figures 3.17 and 3.18 are generated. As can be seen, increasing the fluid level also the roll angle increases.

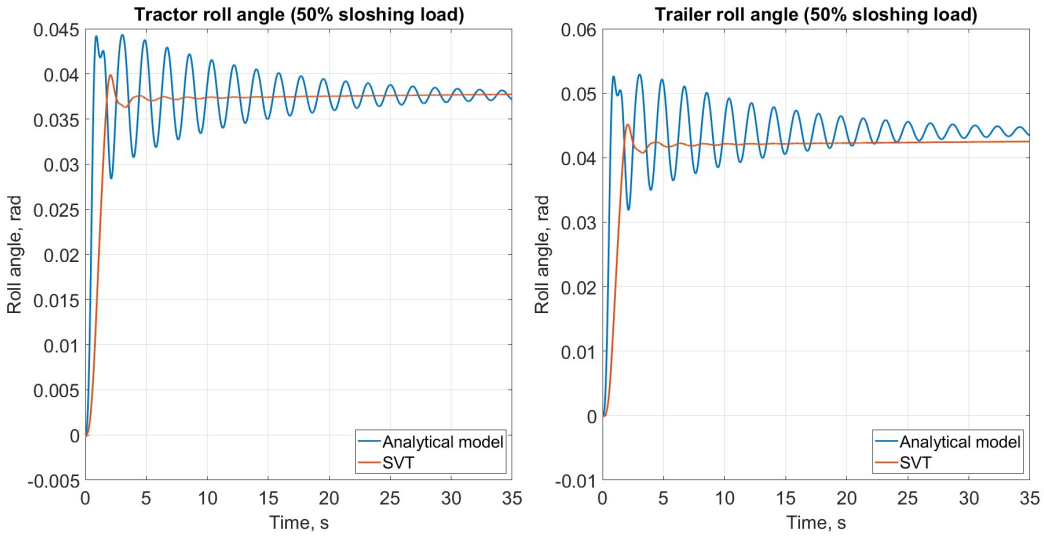

Figure 3.15: Roll angle comparison between analytical and SVT model, with sloshing load (50 %).

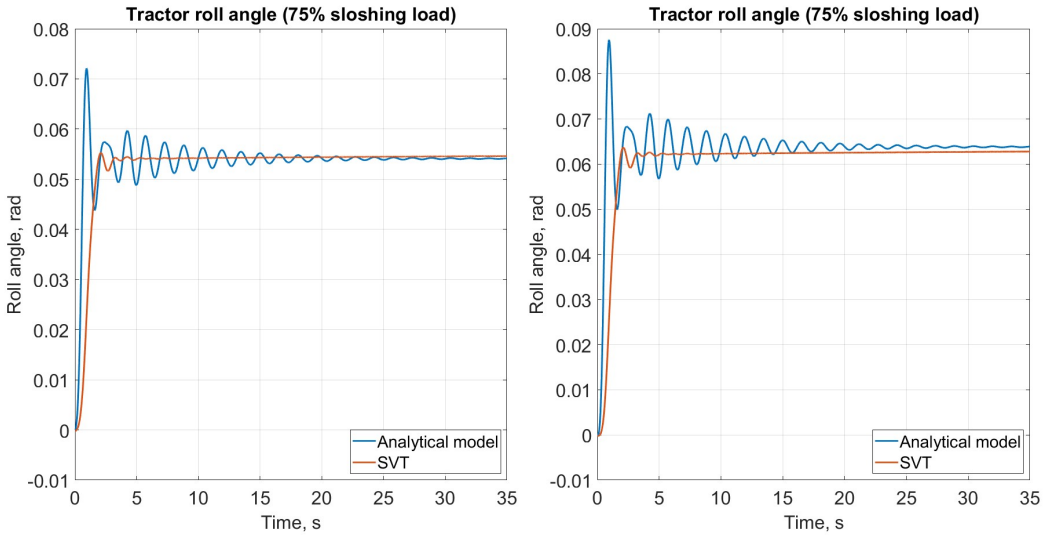

Figure 3.16: Roll angle comparison between analytical and SVT model, with sloshing load (75 %).

Increasing the filling level, the fluid centre of mass moves upwards and this causes an increment of roll angles. It is interesting to notice that when the liquid level is high, the vehicle reaches the maximum roll angle faster than low level filled tanks. Remembering the normalized roll angle introduced in section 3.1, it is possible to

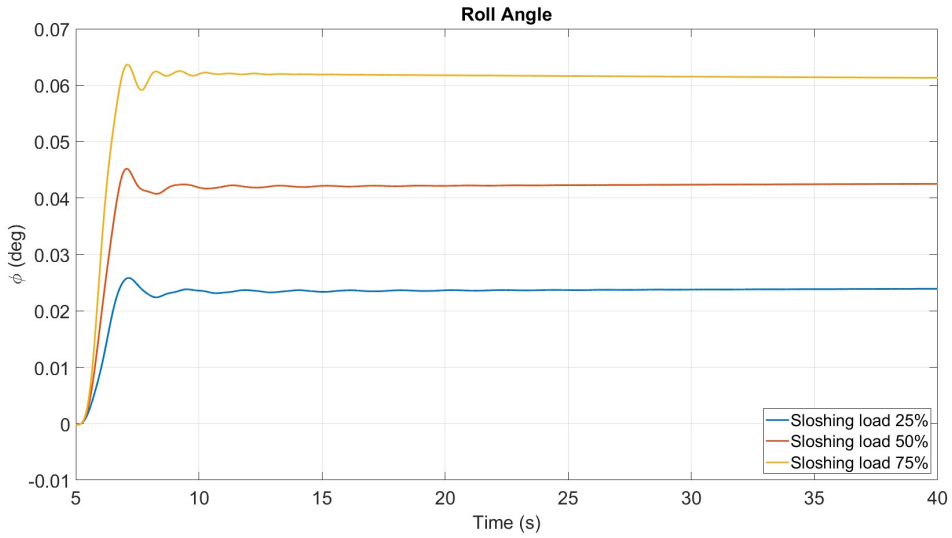

Figure 3.17: Trailer's roll angles with different fluid levels percentage.

observe in Figure 3.18 that oscillations are big at start, where sloshing phenomenon has more impact. Then the vehicle tends to stabilize around its nominal roll angle. Since the roll angle of sloshing load is bigger than equivalent rigid one at steady state, N_ϕ at equilibrium reaches a value greater than 1, depending on the amount of load. It is now clear why sloshing is more dangerous when the tank is almost empty. In fact, when the load is at low level, the sloshing mass is the greatest part. In this way the difference between sloshing and rigid load are evident. It is worth to look also at Figure 3.19. Here the lateral acceleration of tractor and semi-trailer is plotted. The centre of gravity acceleration shows low correlation with sloshing both in tractor and in semi-trailer.

Since SVT model is now validated, an other different manoeuvre has been simulated: the single lane change. It is a manoeuvre where the driver change the lane, for example to overtake an other vehicle on highways or to avoid an obstacle. Driver's input used for simulation are shown in Figure 3.20. The vehicles runs at 60 km/h while the steering angles at the wheels are 2°. Also here, looking at roll angles in Figure 3.21 it is possible to see how sloshing influence negatively vehicle lateral dynamic since it increases the possibility of overturning.

Performing this simulation for different filling levels, it is expected similar results to those obtained with step-steer. In fact, looking at Figure 3.22, increasing the fluid amount, trailer roll angle increases. Anyway, at low levels the trailer tends to oscillate more and takes more time to reach steady-state after the manoeuvre has ended, due to sloshing.

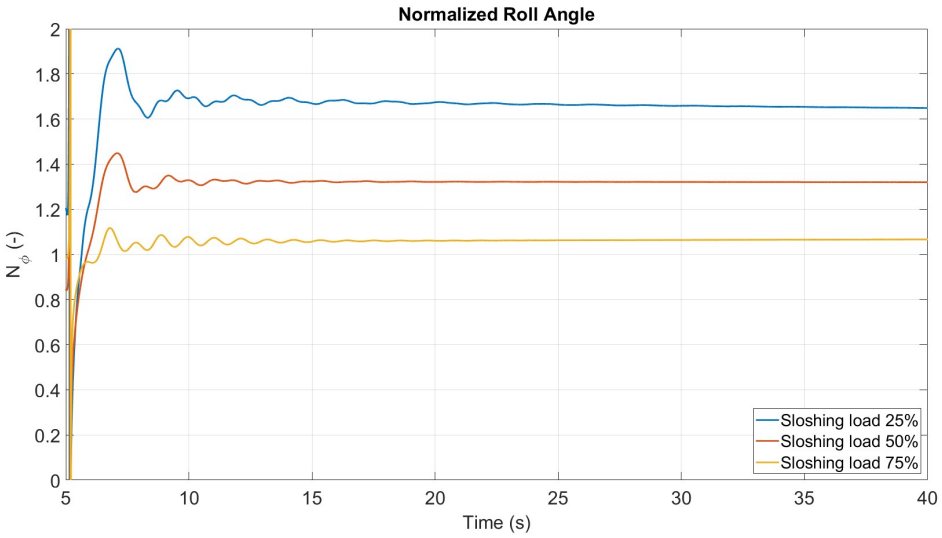

Figure 3.18: Normalized roll angle with different fluid levels percentage.

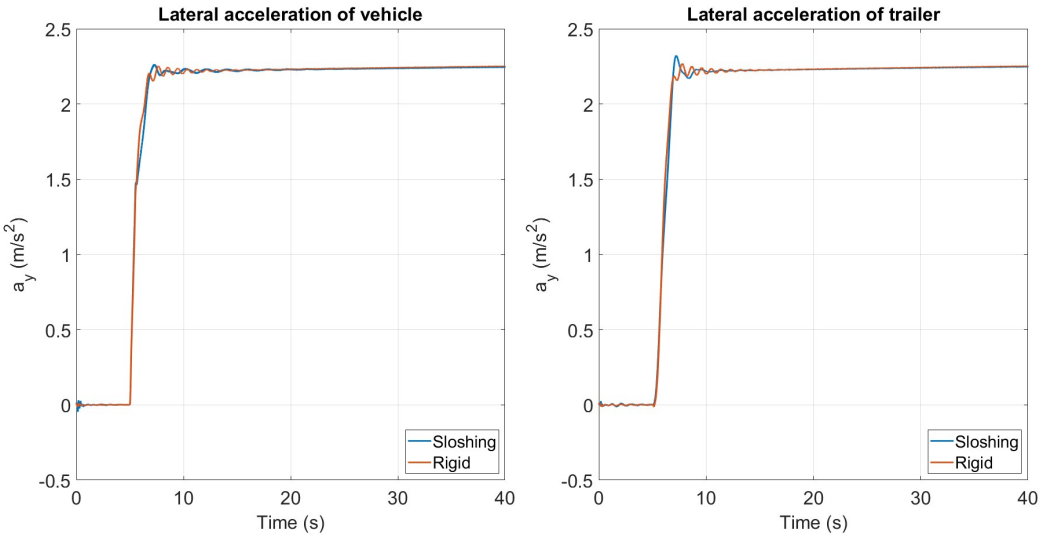

Figure 3.19: Lateral displacement of tractor and trailer with 50% load.

3.3.5 Frequency analysis

In order to understand how the system behaves, a study of system's eigenvalues during step-steer manoeuvre can be carried on. In general, a system is stable if its eigenvalues are complex with negative real part, while it is unstable if the eigenvalues are complex with positive real part. These eigenvalues are the roots

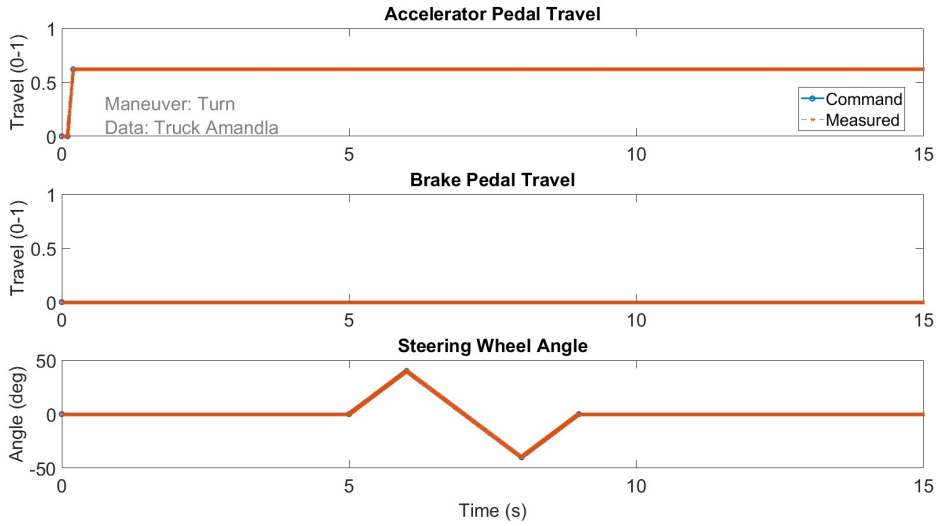

Figure 3.20: Single lane change driver's inputs.

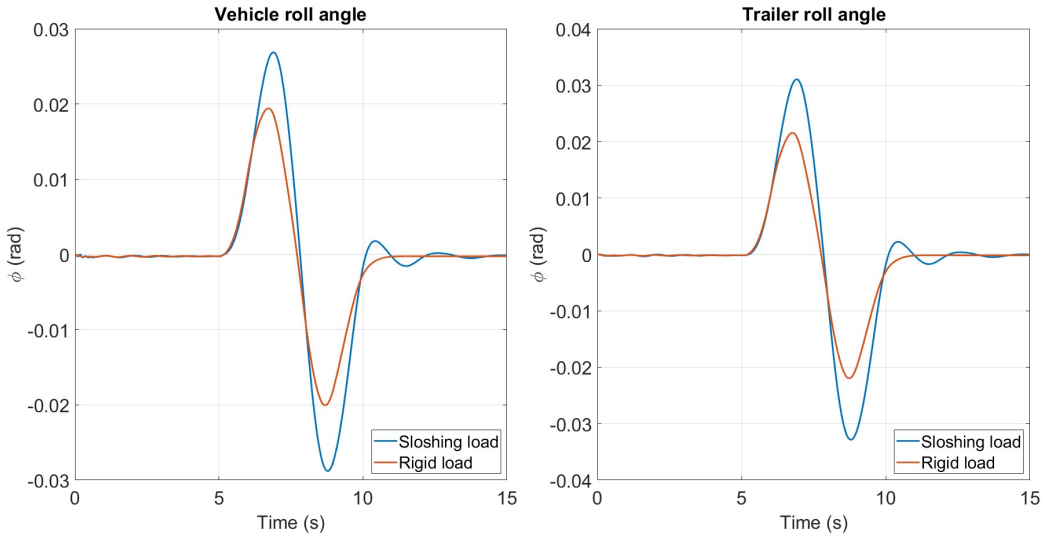

Figure 3.21: Tractor's and trailer's roll angles during single lane change manoeuvre.

of the characteristic equation of the system, which in this case have been obtain using a Matlab function called *damp*.

This kind of analysis allows to observe how the stability changes when one parameter varies. Looking at Figures 3.23 and 3.24, it can be seen how the eigenvalues change when the constant longitudinal speed of the vehicle is modified.

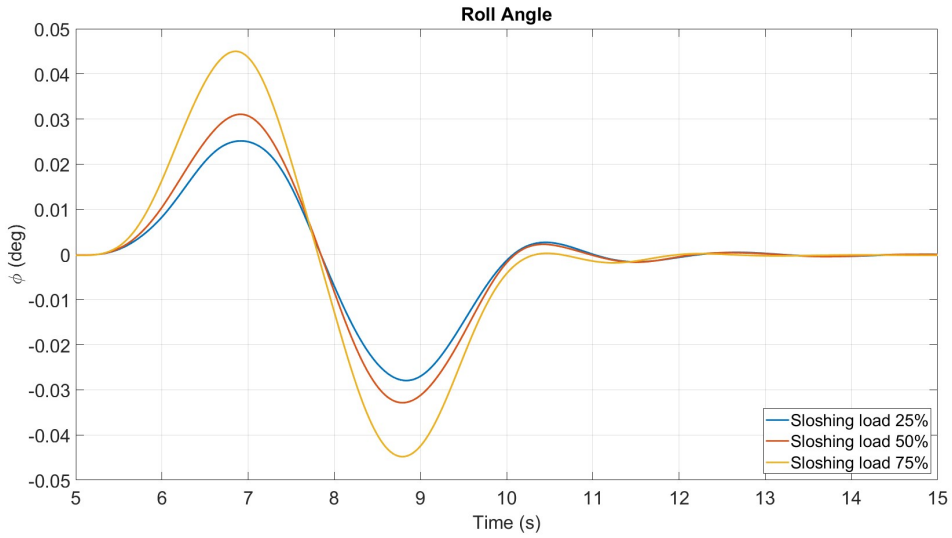

Figure 3.22: Trailer's roll angles during single lane change manoeuvre with different filling levels.

Since not all the value are on the real axis, the systems presents an oscillating behaviour, also at low speeds. Increasing the speed, the poles moves towards the vertical imaginary axis, meaning that the oscillating behaviour is increasing. Comparing the poles at 50 % and 75 % it can be noticed that, in the high filling level some points are closer to imaginary axis, meaning that increasing the payload, also the oscillations increase.

In Figures 3.25 and 3.26 a detailed view of poles for rigid and sloshing load is presented. When the payload is liquid, poles tends to be closer to imaginary axis and moreover, some new points now appears very close to this axis. This indicates a more oscillating behaviour of the system. Same kind of analysis can be done when the liquid level is modified.

Looking now at Figures 3.27 and 3.28, some additional considerations can be said. First of all, at low frequency and low damping ratio, there is an horizontal line: this represents the sloshing frequency and the sloshing damping ratio. It does not change if the vehicle's speed increases, since it depends on tank's geometry. Instead, tractor and trailer behaviour does change with velocity. At increasing speed, tractor's damping seems to decrease, while trailer's one first increases and then, after a certain velocity, decreases. A particular consideration must be done when the liquid level is at 75 %. Looking at damping ratio, at high speed, instability occurs. In fact here the value becomes negative which does not have physical meaning.

Other interesting considerations can be done observing the bode plots of tractor's

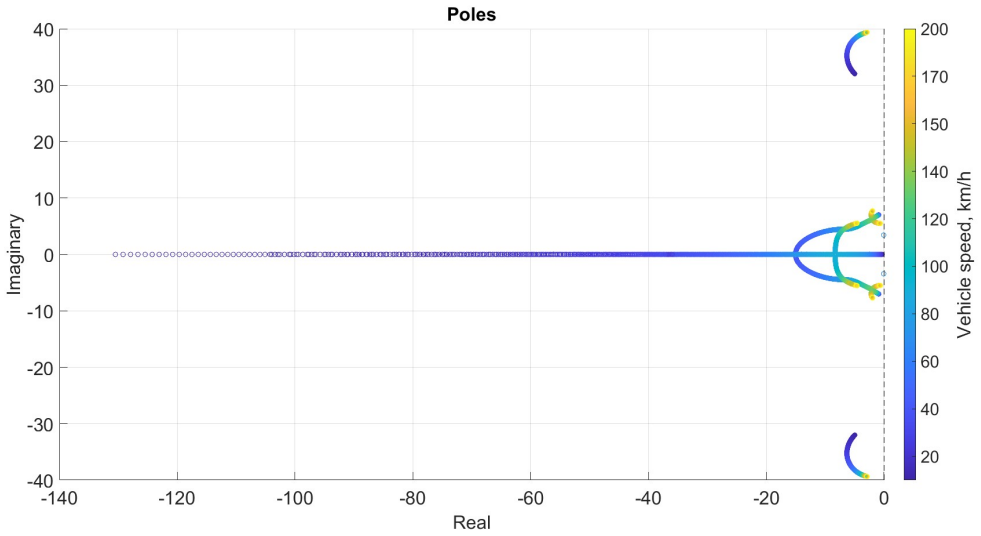

Figure 3.23: System's root locus when tank is filled at 50 %

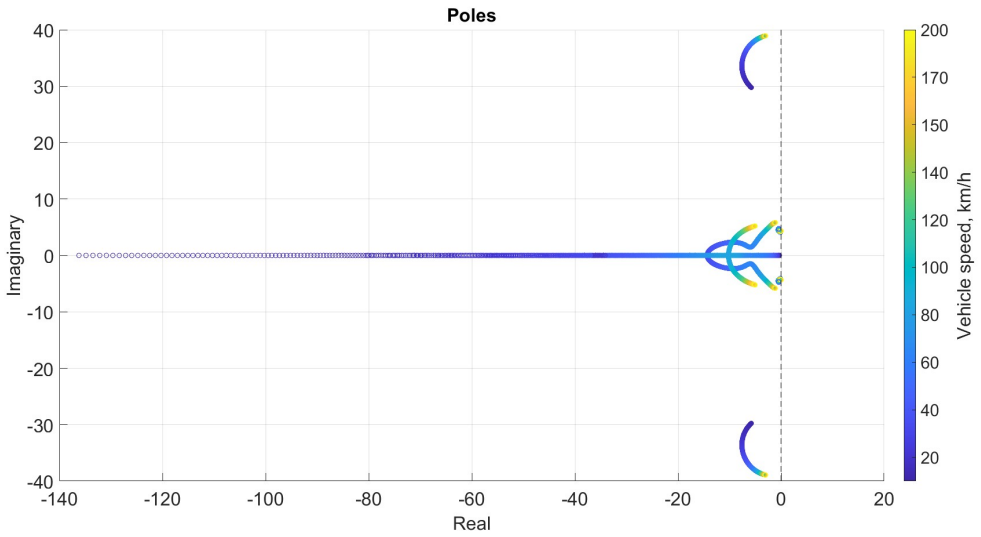

Figure 3.24: System's root locus when tank is filled at 75 %

and trailer's roll angles at 60 km/h, as shown in Figures 3.29 and 3.30. In particular, looking at the magnitude, a large peak is clearly visible at 0.546 Hz, due to sloshing motion. This shows again how sloshing can greatly influence vehicle's lateral dynamic, especially regarding the trailer. Moreover, this explains why sloshing phenomenon is so dangerous, since most of common manoeuvres can range in this natural frequency window. Comparing the 50 % and 75 % cases, it possible to see

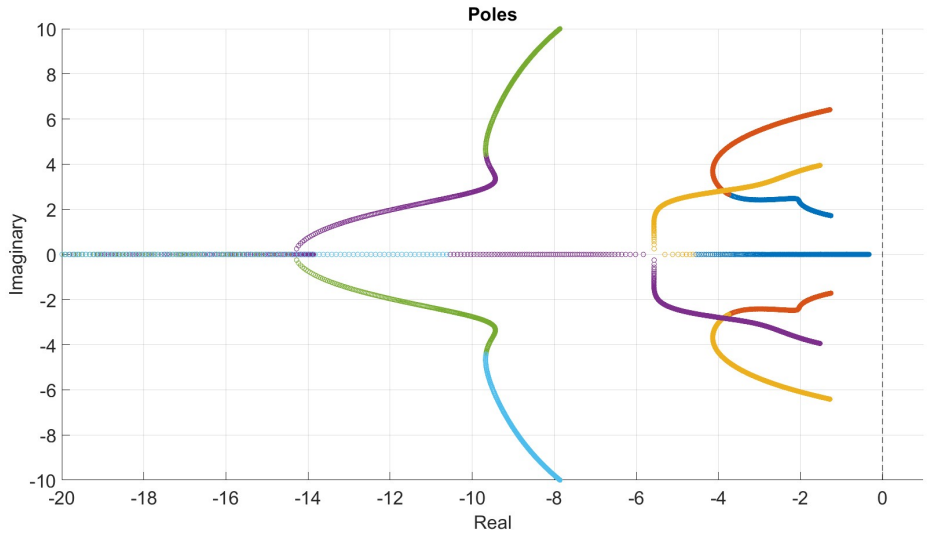

Figure 3.25: System's root locus when tank is filled at 50 % with a rigid load (detail view).

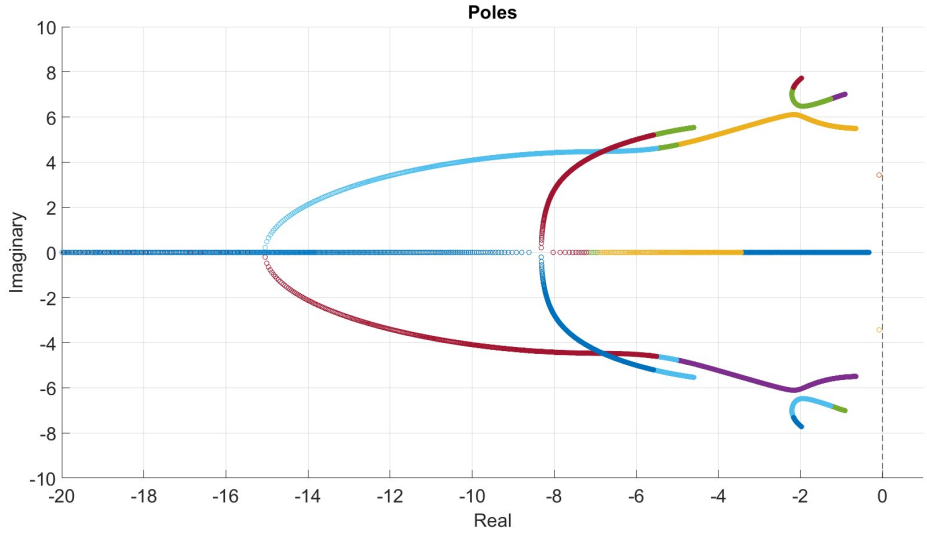

Figure 3.26: System's root locus when tank is filled at 50 % with a sloshing load (detail view).

how the sloshing motion influence the magnitude more in the first case, since the sloshing mass is bigger in 50 % case than 75 % one. In the figures, two more peaks can be noticed. They are related to suspensions and tire characteristics.

One way to check if analytical results are correct, is the analysis of the sloshing

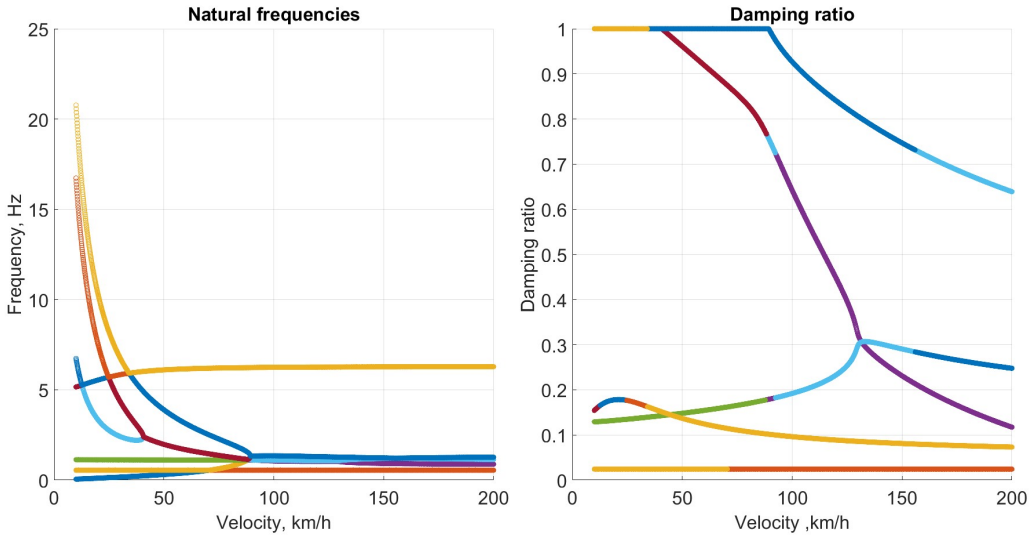

Figure 3.27: Natural frequency and damping ratio of the system (50 % sloshing liquid).

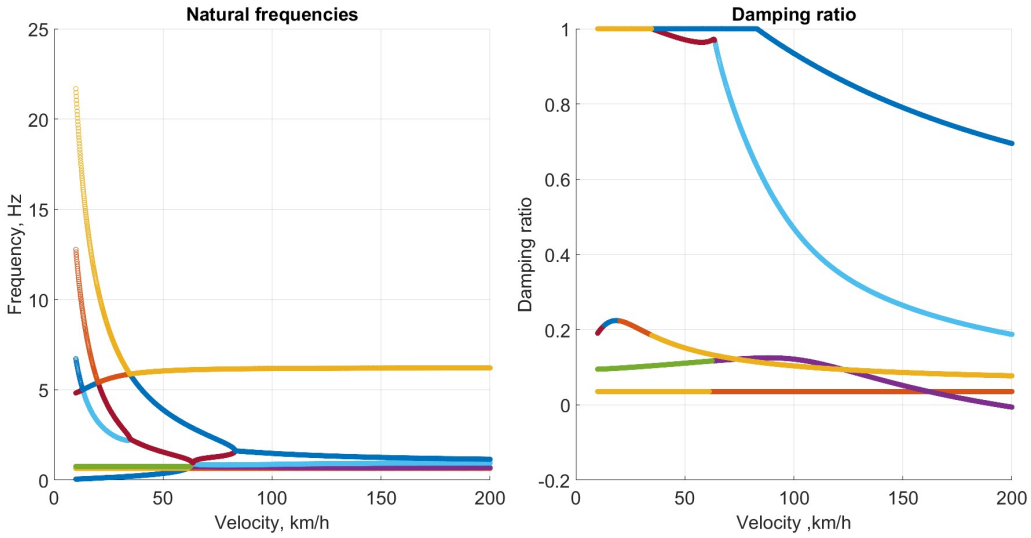

Figure 3.28: Natural frequency and damping ratio of the system (75 % sloshing liquid).

natural frequency. As said previously, it is possible to calculate the natural frequency of the equivalent mechanical model through the equation 3.34. The curve representing the natural frequency independently from the tank's geometry is shown in Figure 3.31, where first mode in case of lateral sloshing is plotted

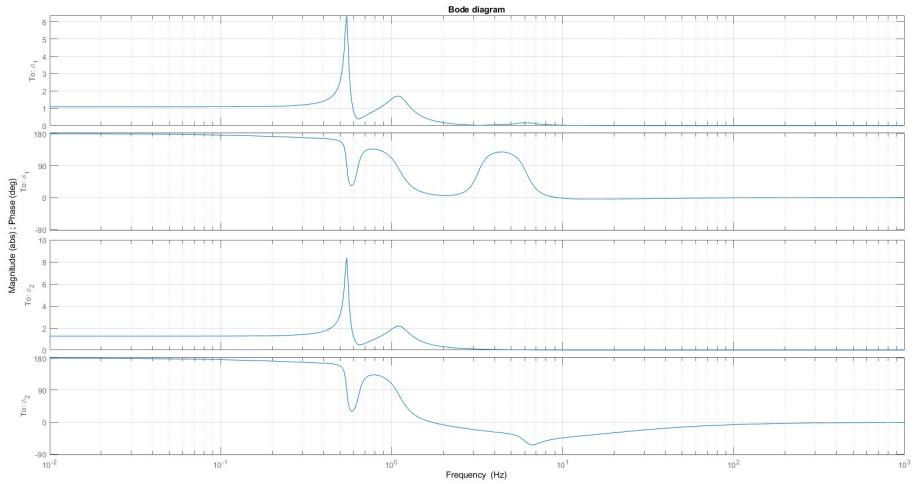

Figure 3.29: System's bode plot when tank is filled at 50 %

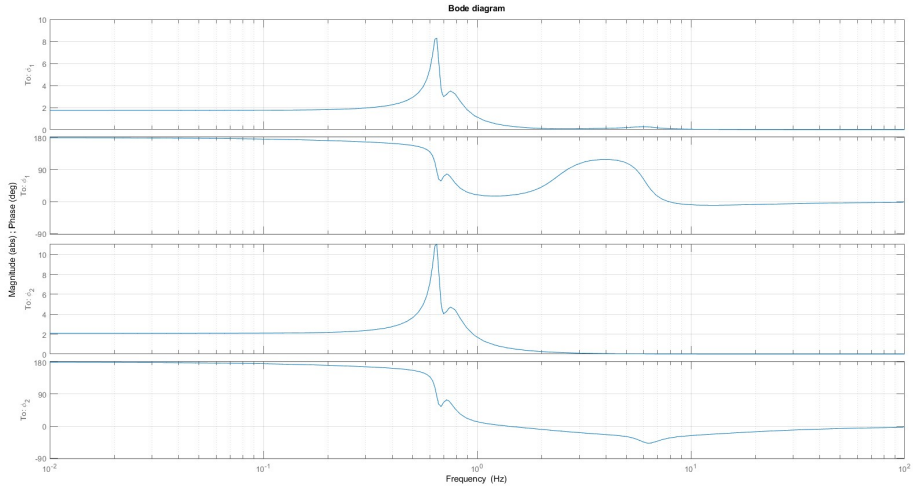

Figure 3.30: System's bode plot when tank is filled at 75 %

against the filling percentage. Since the first mode is the most important one, other orders have been neglected for this analysis. In the same Figure, on the right side there are some experimental results. What can be noticed is that the natural frequency increases with the filling level, and it can be observed also when comparing bode plots (Figures 3.29 and 3.30). Anyway, when increasing the liquid level, the amplitude of oscillations decreases.

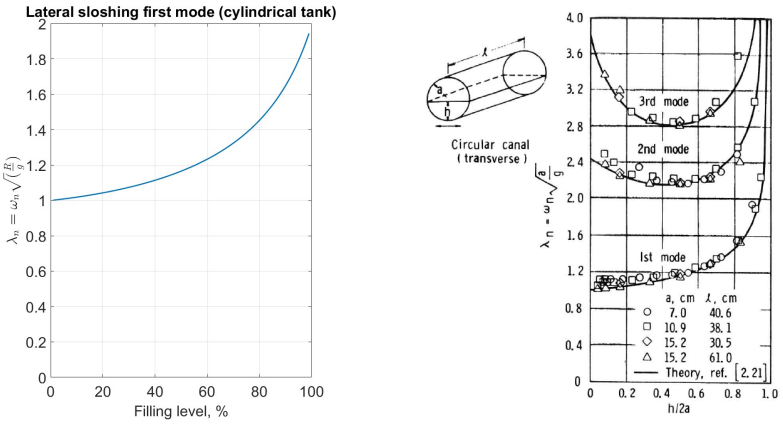

(a) Analytical model **(b)** Experimentally determined

Figure 3.31: Variation of natural frequency parameter of analytical model (a) and experimentally determined (b), [13].

Chapter 4

Longitudinal sloshing

4.1 Braking manoeuvre

Sloshing event can be important not only when analysing the vehicle's lateral dynamic, but it has also a considerable effect on longitudinal dynamic. Even if it is not source of catastrophic events such as roll-over, the sloshing can become a problem during braking manoeuvre. In fact, a sudden deceleration forces the fluid inside the tank to move, causing an increase of total braking distance. The situation is even worse if the braking event is not performed in perfectly linear condition, where it becomes a problem also for what concerns the lateral dynamic.

Since the complexity of the problem can be quite high, common practice to study the longitudinal sloshing is through numerical approach or by means of Euler-Lagrange analytical solution. Jalili et al. [14], analysed a tractor and trailer system carrying a liquid load solving numerically Euler and Laplace equations. What they found out is that the sloshing influence the braking distance, depending on various factors.

The most important one is the filling level: with the increasing of the filling level, the liquid cargo behaves more like a rigid one. Low liquid levels increases the sloshing effect, and this results can be seen looking at the normalized velocity and normalized pitch angle. Normalized velocity of the semi-trailer is defined as the ratio between the vehicle's speed when carrying liquid and when carrying an equivalent rigid cargo. As can be noticed in Figure 4.1, when the tank is almost filled up, the normalized speed is lower than when the fluid level is low, meaning that the vehicle takes more time to stop in presence of sloshing. These results are confirmed when looking at trailer's pitch angle (Figure 4.2). Here the normalized pitch angle, defined as the ratio of pitch angle of liquid load and rigid one, is plotted. Those big oscillations cause the change on the vertical load of the axles which greatly influences the breaking performance.

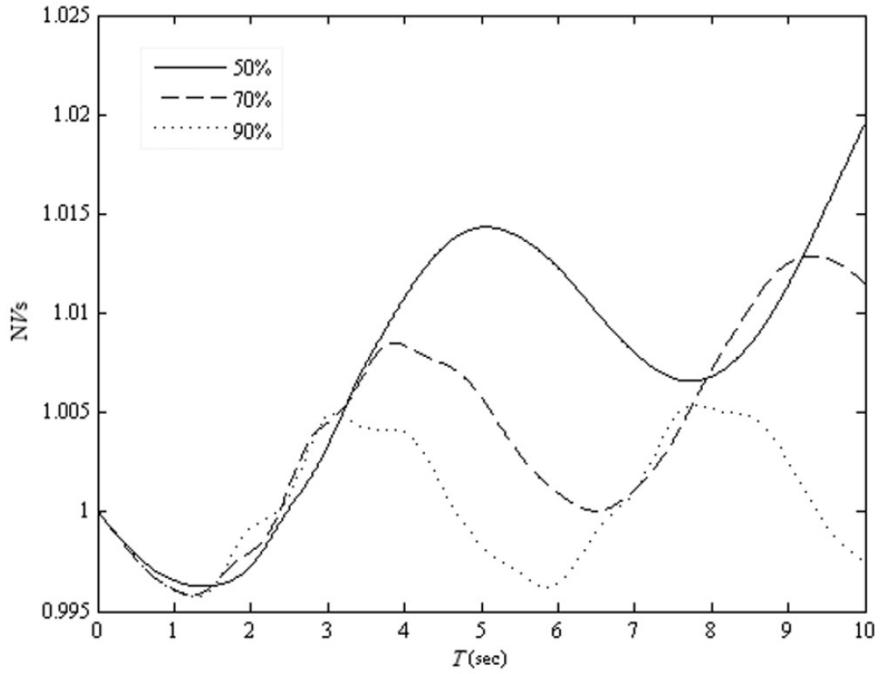

Figure 4.1: Normalized velocity of the semi-trailer at different load levels, [14].

In [14] is also taken in consideration a change of liquid density. The more dense is the liquid load, the more it will behave as a rigid one, so as expected the sloshing effect with low density liquids is more evident, even if it has less impact on vehicle's dynamic than filling level.

Yan and Rakheja [15] studied the longitudinal sloshing in an other type of tank truck with the aim to understand the effectiveness of baffles inside the tank. Anyway, some results can be still taken in consideration to understand the sloshing dynamic. Looking in Figure 4.3, it is possible to see how pitch angle and vertical sprung mass displacement changes in case of rigid and liquid load. During a braking manoeuvre, the vehicle's sprung mass moves considerably along vertical axis, which leads to a change also in the axis load, and so affecting the braking performance. This behaviour can be appreciated looking also at Figure 4.4, where longitudinal speed and acceleration are shown.

4.2 Equivalent mechanical model

In few studies, longitudinal sloshing is analysed by means of equivalent mechanical models, such as mass-spring or pendulum's one.

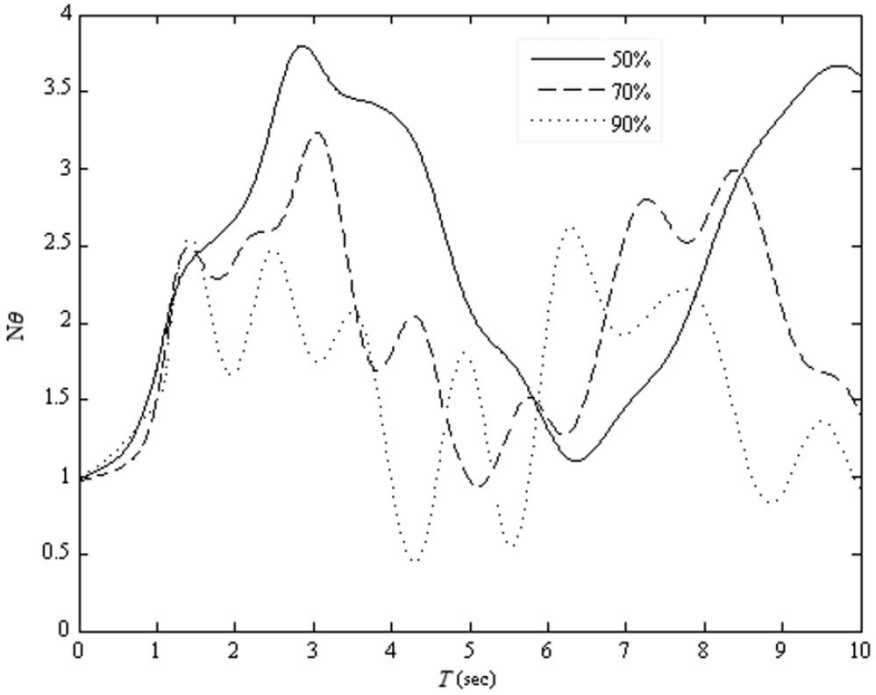

Figure 4.2: Normalized pitch angle of the semi-trailer at different load levels, [14].

Godderidge et al. [5] used the pendulum model to simulate the sloshing phenomenon in a rectangular tank. They showed how to obtain the effective sloshing mass analytically for a rectangular tank. In case of different geometry, the pendulum's mass can be obtained experimentally exciting the tank with an harmonic motion at a frequency lower than the natural one. Then the motion is stopped and the maximum force measured right after this moment is considered for the calculation as follow:

$$m = \frac{F_{max}}{x_0}\left(\frac{1}{\omega^2} - \frac{1}{\omega_n^2}\right) \tag{4.1}$$

where x_0 is the tank displacement, ω is the exciting frequency, ω_n is the natural frequency.

Anyway, there is no empirical formulas to calculate the natural frequency of longitudinal sloshing. Also in this case, experiments must be done. In [13], experiments of this type have been done for different tank's geometries. For example, considering a cylindrical tank, the results shown in Figure 4.5 allow to obtain the natural frequency of the longitudinal sloshing independently from tank's dimensions.

In recent studies Li et al. [16], developed a mechanical analogy based on mass-spring model of sloshing in rectangular tanks. In particular, the main model's

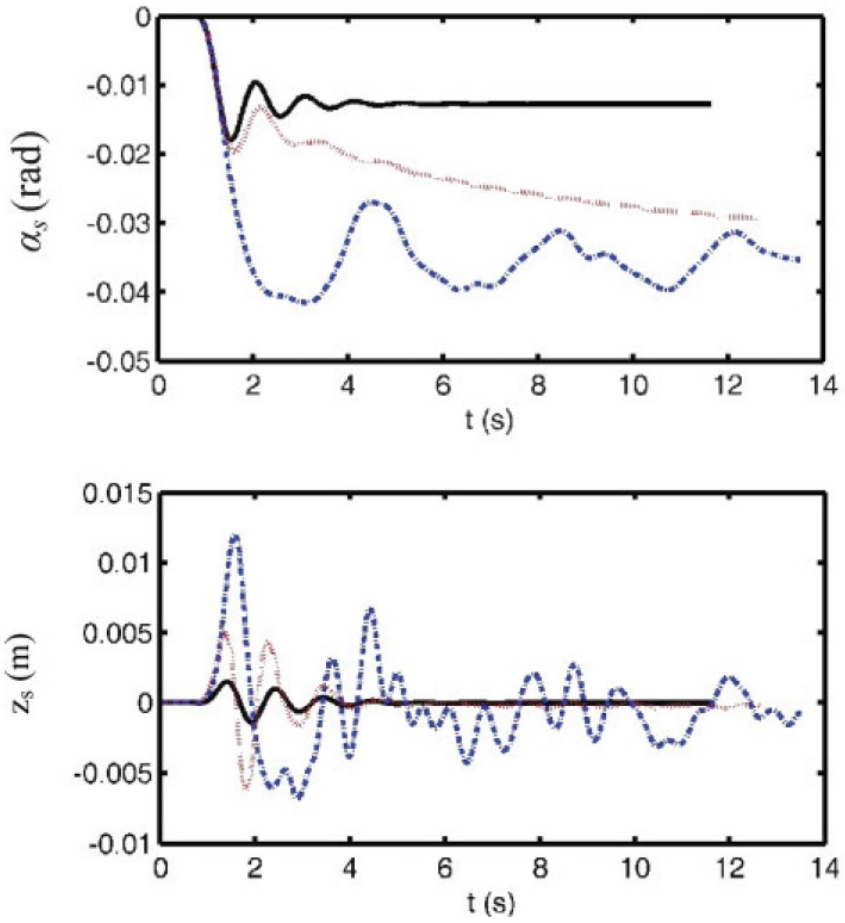

Figure 4.3: Pitch angle and sprung mass vertical displacement in case of rigid load (solid black line), liquid unbaffled load (blue dotted line), liquid baffled load (red dotted line), [15].

parameters can be expressed as in the following:

$$M_n = M \frac{2(H/l)^2 \tanh(\beta_n H)}{(\beta_n H)^3} \tag{4.2}$$

$$h_n = H \left(1 + \frac{2 - \cosh(\beta_n H)}{\beta_n H \sinh(\beta_n H)} \right) \tag{4.3}$$

$$M_0 = 1 - \sum_{n=1}^{\infty} \frac{M_n}{M} \tag{4.4}$$

$$h_0 = H \left(\frac{C_1 + C_2}{C_3} \right) \tag{4.5}$$

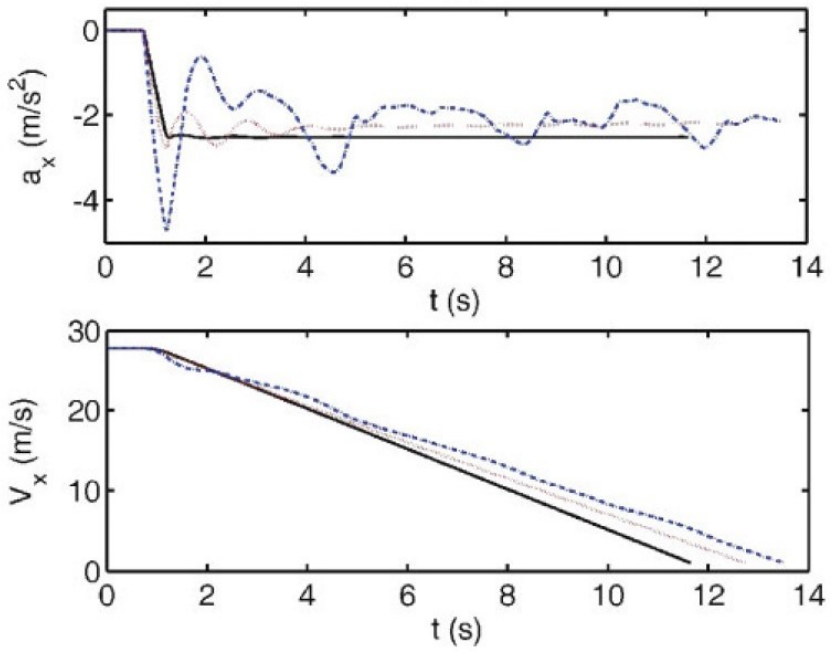

Figure 4.4: Longitudinal acceleration and velocity in case of rigid load (solid black line), liquid unbaffled load (blue dotted line), liquid baffled load (red dotted line), [15].

$$K_n = M_n \omega_n^2 \tag{4.6}$$

where M is the total fluid mass, M_n is the sloshing mass, M_0 is the fixed mass, H is the fluid height, h_n is the sloshing mass height, h_0 is the fixed mass height (all the heights are measured from tank's bottom to liquid free surface), l is the tank's half-length, K_n is the equivalent spring stiffness, ω_n is the natural frequency. While all the other variables are so defined:

$$\beta_n = \frac{(2n-1)\pi}{2l} \tag{4.7}$$

$$\omega_n = \sqrt{g\beta_n \tanh(\beta_n H)} \tag{4.8}$$

$$C_1 = \frac{1}{2} + \frac{1}{3}\left(\frac{l}{H}\right)^2 \tag{4.9}$$

$$C_2 = -2\left(\frac{H}{l}\right)^2 \sum_{n=1}^{\infty} \frac{2 + \beta_n H \sinh(\beta_n H) - \cosh(\beta_n H)}{(\beta_n H)^4 \cosh(\beta_n H)} \tag{4.10}$$

$$C_3 = 1 - \sum_{n=1}^{\infty} 2\left(\frac{H}{l}\right)^2 \frac{\tanh(\beta_n H)}{(\beta_n H)^3} \tag{4.11}$$

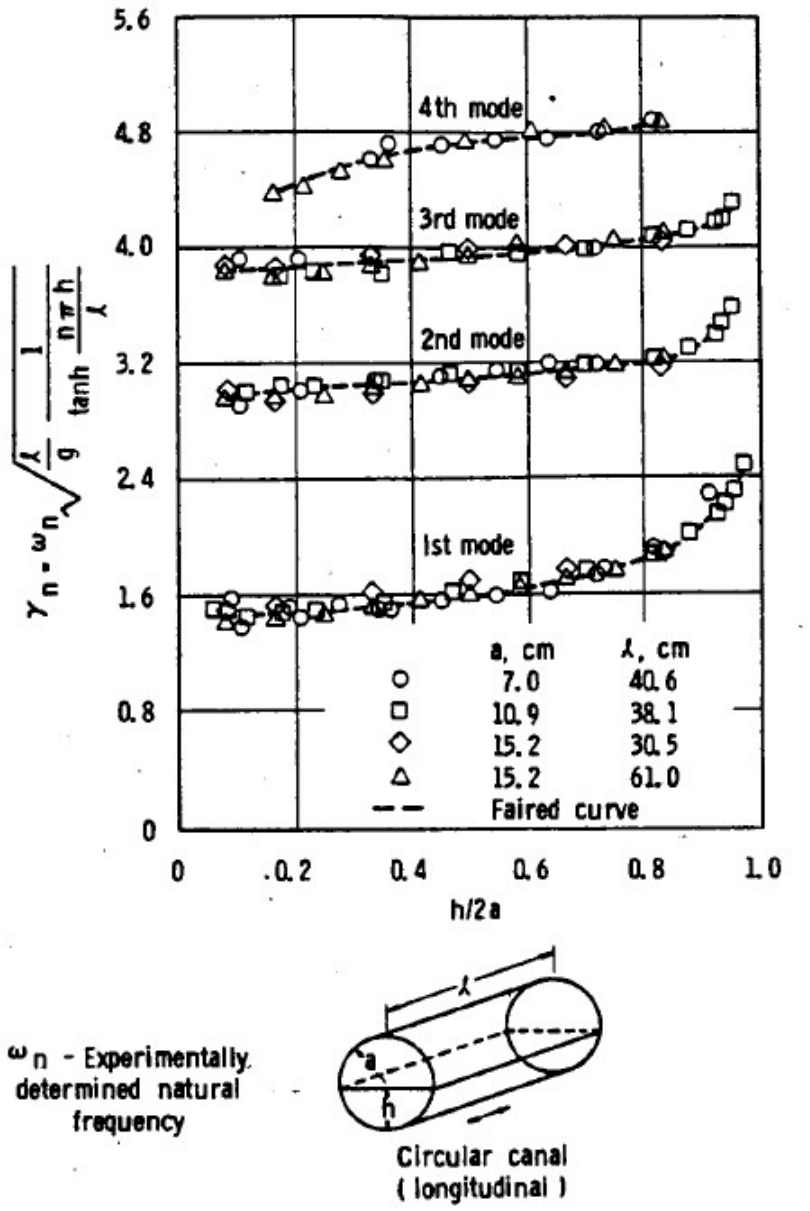

Figure 4.5: Natural frequency parameter in function of liquid depth, [13].

Since there is not a rigorous formulation for longitudinal sloshing in horizontal cylindrical tanks, Ranganathan et al. [17] simplified the problem subdividing the circular area in n rectangles. In this way, equations 4.2 through 4.11 can be used to compute the mechanical model in each element. Taking Figure 4.6 as reference,

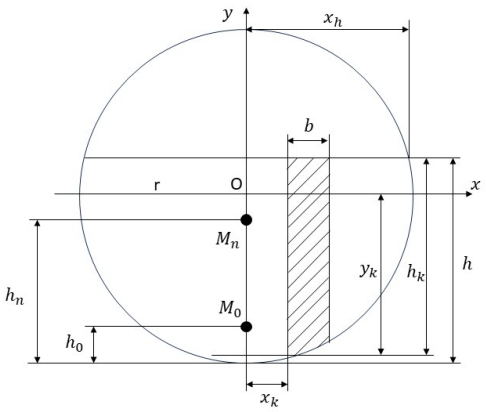

Figure 4.6: Dimension of each element of cylindrical tank, [17].

each k element's coordinates can be written as:

$$x_k = (k-1)b; \qquad y_k = R\sqrt{1 - \frac{(k-1)^2}{n^2}}; \qquad \text{for} \quad k = 1, 2, ..., n \tag{4.12}$$

and the total element height as:

$$h_k = y_k + (H - R) \qquad \text{for} \quad k = 1,2, ..., n \tag{4.13}$$

where $b = R/n$ is the width of each element, n the total number of element and R the tank's radius. Errors due to this approach are minimal when a large number of elements is taken into account, anyway also with 10 of them is possible to have a good accuracy. Since the geometry is specular, only one half of the tank is considered, and then with a summation process is possible to obtain the entire tank's parameters.

This mechanical model is then compared with experimental results shown before in Figure 4.5, and result is presented in Figure 4.7. As can be noticed, the mechanical model is quite accurate in predicting the natural frequency of the longitudinal sloshing when filling levels between 30 % and 80 % are considered. Outside this interval the model is not capable of give correct results.

Since there is not a proper formulation for cylindrical tanks, it is difficult to insert in this kind of model a damping ratio. In case of longitudinal sloshing, the fluid impacts against the front and rear walls creating a non-linear effects which is difficult to represents with these simple models. Anyway, in a braking manoeuvre,

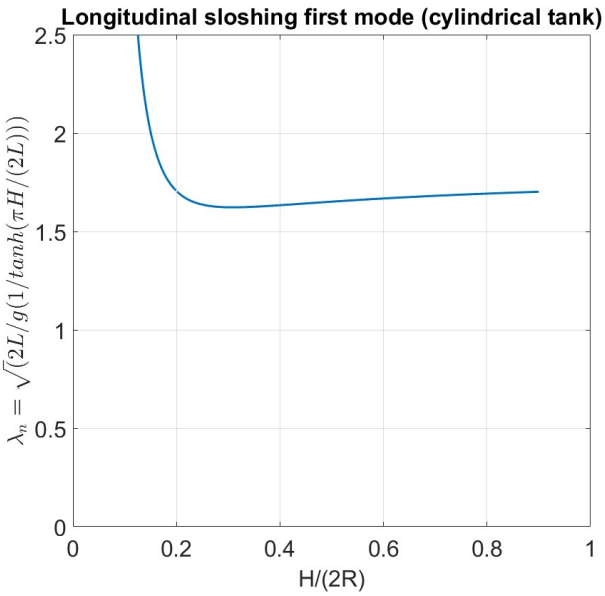

Figure 4.7: Longitudinal sloshing non-dimensional natural frequency in a horizontal cylinder.

if the deceleration is quite small (around 0.1 g) non-linear effects are not present and the system can be analysed also in absence of damping.

Starting from natural frequency, it is possible to transform the spring-mass model in a pendulum one. Since the pendulum's frequency can be written as function of rod length, it can be obtained through:

$$l_{pend} = \frac{g}{\omega_n^2} \tag{4.14}$$

where l_{pend} is the pendulum's rod length, g is the gravity acceleration and ω_n is the natural frequency calculated with equation 4.8. Then the hinge position can be easily derived from oscillating mass position calculated in equation 4.3 and rod length.

4.3 Model validation

The main problem of the mechanical sloshing described in section 4.2 is that it has been developed for not too shallow tanks. This creates some problems during the computation of sloshing and fixed mass positions, especially at low filling levels, when the filling height to tank's length ratio is very low.

For this analysis the reference [18] is considered, where sloshing in cylindrical tank with and without baffles are simulated. Taking into account only clean bore tanks,

SVT simulations can be validated. Modaressi-Tehrani et al. performed sloshing simulations with two different filling levels (40 % and 60 %) and accelerations (0.3 g and 0.6 g) on a tank 7.55 m long with a diameter of 2.03 m (list of data in Table 4.3). Since the mechanical model presented is not able to sustain high longitudinal acceleration, just 0.3 g has been analysed in Simscape.

Starting from the mean longitudinal force developed during the braking event, it is possible to notice that mechanical model and Simscape gives comparable results, as shown in Table 4.1. These results confirm the accuracy of mechanical model to describe the amount of sloshing mass and of the fixed one. Main discrepancies are due impossibility to obtain exact trailer's deceleration, especially at low liquid percentage. These values can be alternatively obtained multiplying the sloshing mass with the desired longitudinal acceleration.

Table 4.1: Mean longitudinal force at 0.3 g.

Filling level	Reference [18]	Pendulum
40 %	22,298 N	17,498 N
60 %	37,261 N	30,545 N

In order to check the dynamic response, the amplification factor M_{R_p} is introduced. It is defined as the ratio between the maximum value and the mean one. In this case the parameter taken in consideration is the longitudinal acceleration:

$$M_{a_x} = \frac{\max(a_x)}{\bar{a_x}} \tag{4.15}$$

where a_x is the longitudinal acceleration, while $\bar{a_x}$ is its mean value. Results are shown in Figures 4.8 and 4.9, and summed up in Table 4.2. For the calculation of M_{a_x}, the first peak has been taken into account, neglecting the last moments where the vehicle stops and numerical solution does not give proper values. It is possible to observe how 60 % simulation shows more correct results, in accordance with the reference values, while at lower filling level there are some problems. In Figure 4.8, at about 9 s, there is a large peak due to vehicle instability. Here in fact, the trailer tends to detach from the ground, and consequently experiences a large acceleration. This event is due to the unlimited motion of the pendulum. In real world, the fluid motion stops when reaches the front tank wall, generating a large wave. Consequently the sloshing becomes non-linear and cannot be represented any more by a pendulum. For this reason the pendulum model can be only used in not too shallow tanks excited with low accelerations.

Introducing now a limit in the pendulum motion, new simulation can be run in order to consider fluid impacts against tank's front wall. This limit has been

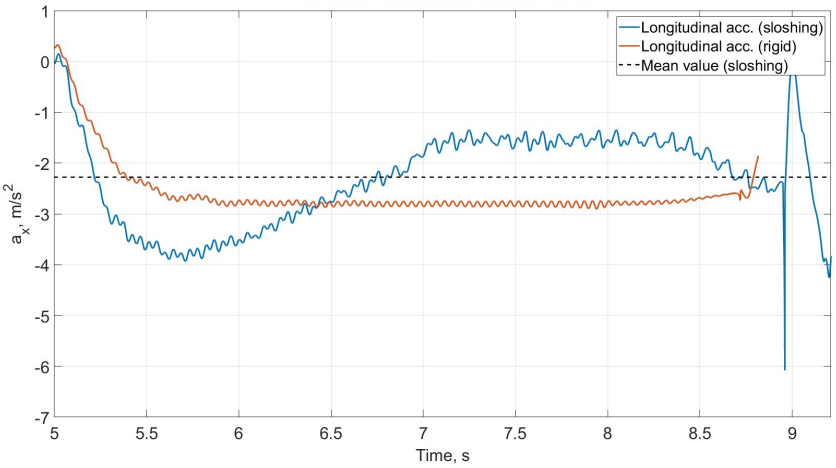

Figure 4.8: Longitudinal acceleration in 40 % filled tank subjected to 0.3 g.

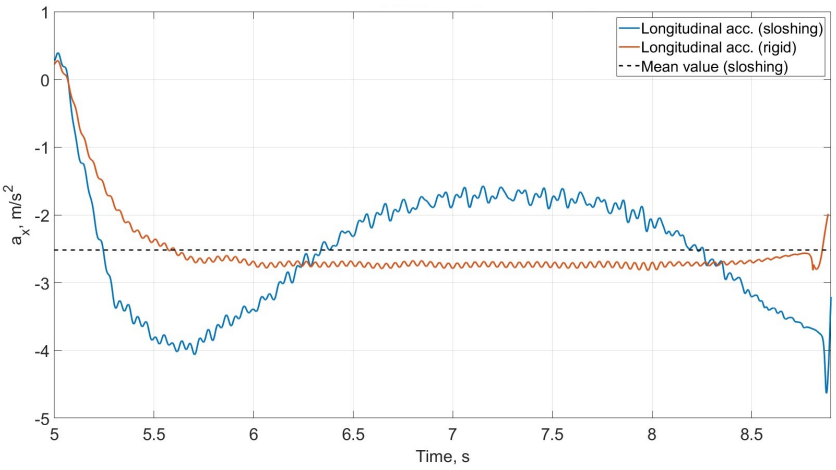

Figure 4.9: Longitudinal acceleration in 60 % filled tank subjected to 0.3 g.

imposed limiting the maximum angle displacement around pendulum's rotational axis at a value depending on hinge location and rod length. The results for 40 % and 60 % are shown in Figures 4.10 and 4.11. Observing the results obtained in case of low filling level, it is clear that impacts have large influence on longitudinal sloshing even if a proper impact model is not introduced. The moment in which the the sloshing mass reaches the maximum longitudinal displacement, a large peak in acceleration and force is recorded. These affects negatively the results, in fact the amplification factor defined in Equation 4.15 now becomes equal to 1.47 at low filling level, a value quite different from the trend observed in Table 4.2. Better

Table 4.2: Amplification factor at 0.3 g.

Filling level	Reference [18]	SVT model
40 %	1.77	1.73
60 %	1.67	1.61

Table 4.3: Vehicle data used in simulation.

Parameter	Value	Units	Description
m_{s1}	5350	kg	Tractor sprung mass
a_1^*	4.827	m	Tractor wheelbase
h_{s1}	1.544	m	Distance of tractor COG from the ground
b_{f1}	1.397	m	Distance between front axle and tractor COG
b_r^*	4.445	m	Distance between hitch and front axle of tractor
$h_{a,r}$	1.250	m	Distance of hitch from the ground
m_{s2}	4903	kg	Trailer sprung mass
a^*	6.000	m	Trailer wheelbase
h_{s2}	1.544	m	Distance of trailer COG from the ground
b_f	3.000	m	Distance between hitch and trailer COG
L	7.550	m	Tank's length
R	1.015	m	Tank's radius

results are noticed in case of 60 %, however also in this case, the amplification factor is different from before, and becomes 1.46 due to sloshing impacts.

In conclusion, the pendulum mechanical model is a good alternative which offers low computational effort but with also big disadvantages. In fact, certain ranges of fluid level cannot be computed and the deceleration must not be excessive to avoid non-linearities. Moreover, the limit imposed to simulate impacts on front wall introduces complexity to the model and sometimes leads to incorrect results. Anyway, it is needed in order to avoid larger problems related to lifting of trailer when the sloshing mass goes too much out boundaries determined by tank's geometry.

Since this mechanical model is completely different from the lateral one, the

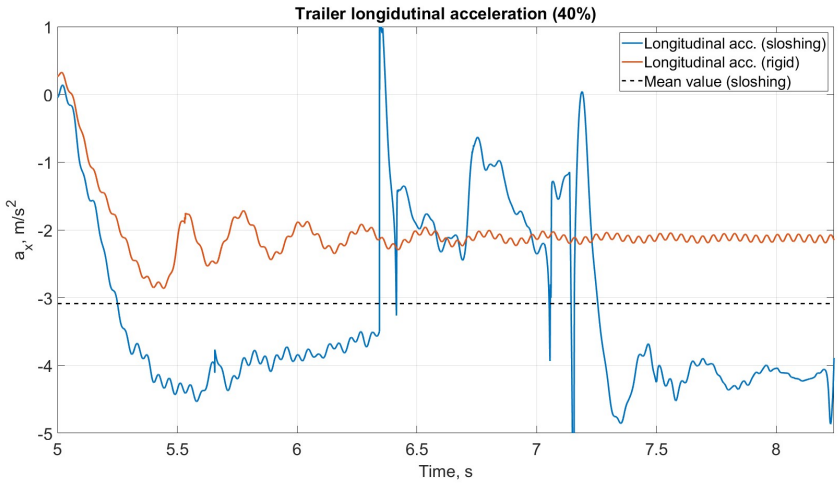

Figure 4.10: Longitudinal acceleration in 40 % filled tank subjected to 0.3 g with impacts simulation.

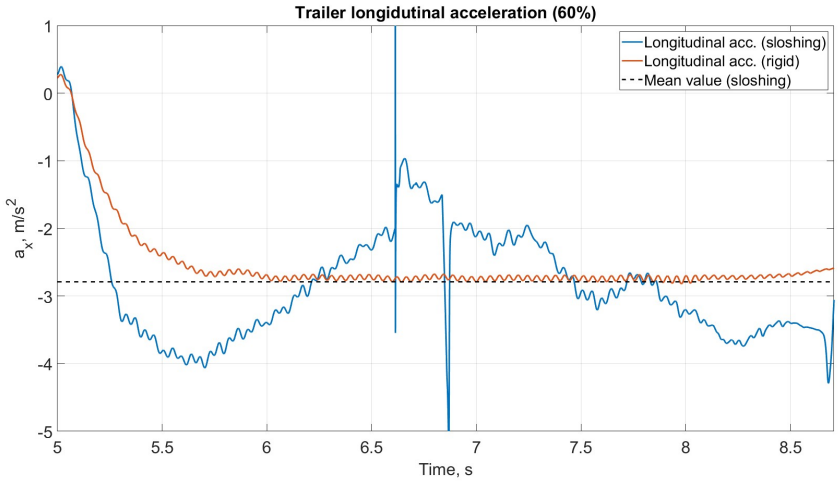

Figure 4.11: Longitudinal acceleration in 60 % filled tank subjected to 0.3 g with impacts simulation.

longitudinal sloshing developed in this way cannot be coupled with the lateral dynamic. This does not allow further investigation on even more dangerous manoeuvres which comprehends both the use of steering and braking.

4.4 Jack-knife instability

When an articulated vehicle is subjected to heavy braking, there could be instability, especially when related to tractor rear axle. This is the case of jack-knife. It is characterized by a sudden loss of grip of the tractor, also when no input at steering wheel is applied, which force the angle at the hitch to increase. Since it is less problematic than rollover, there are few studies which aim at the detection and control of jack-knife measuring the fifth-wheel angle. In this section the influence of longitudinal and lateral sloshing is studied separately in order to observe how vehicle dynamic changes in presence of liquid.

For the following analysis, reference [19] has been taken into account. Mikulcik presented an analytical study for a generic heavy-duty vehicle, where different steering and braking manoeuvre are shown to be source of jack-knife. In this chapter, the analysis will focus only on the braking event, since it is the most frequent cause of this phenomenon. In Appendix C main vehicle data found in reference are summed up.

Since the jack-knife is caused by a sudden skid of tractor, it is useful to simplify the problem analysing the case when brakes are applied only at rear tractor rear axle. As shown in Figure 4.13, increasing in brake pressure can leads to loss of grip on braking tires, and as consequence to jack-knife, which can be detected through yaw rate. Tire slippage can be observed also looking at Figure 4.12. In

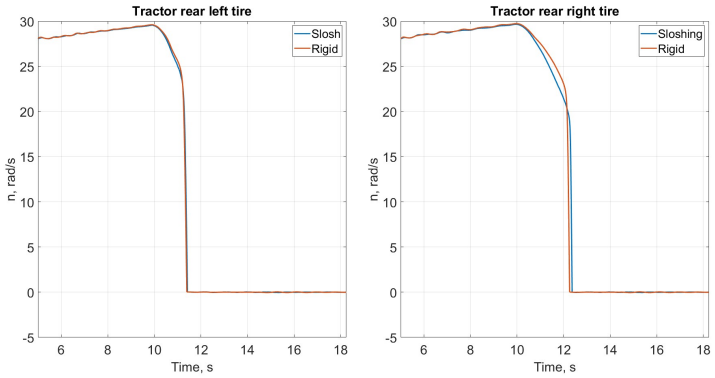

Figure 4.12: Tires speed when tank is filled at 40 % while steering and braking.

this example, results when brakes are applied during steering are shown. For this reason, the inner tire starts to slip first. When also the outer tire begins to slip, tractor yaw rate increase immediately and vehicle becomes unstable and the driver cannot control it any more.

Since lateral and longitudinal models for sloshing are not compatible with each other, the jack-knife problem is analysed separately in two cases.

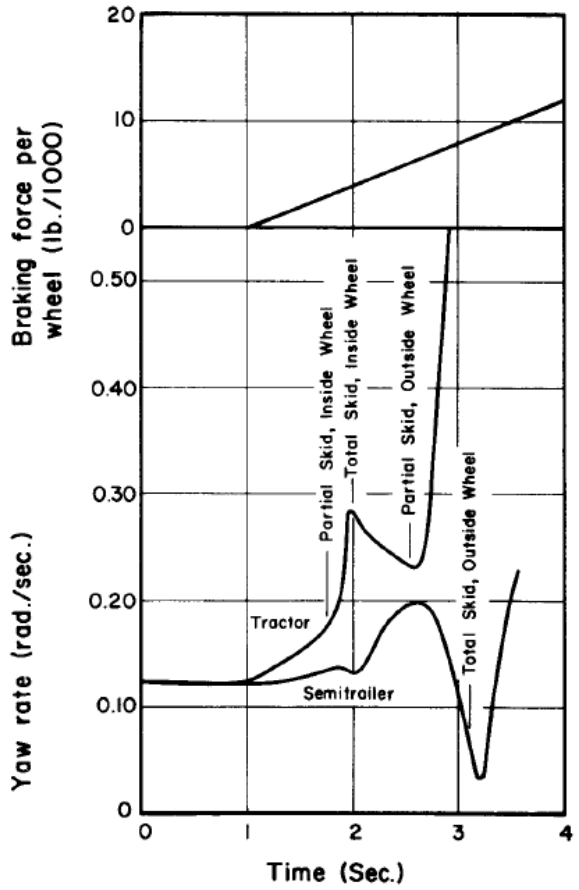

Figure 4.13: Yaw rate during steering and braking only with rear axle, [19].

4.4.1 Jack-knife with lateral sloshing

Since the lateral sloshing is considered, it is possible to simulate a braking during a turn. Referring to Figure 4.13, the vehicle runs at 65.84 km/h and it is turning with a constant angle of 1.43°. Vehicle starts to steer at 5 s and, after the transitory phase, the it starts braking at 10 s, as shown in Figure 4.14. Two different amount of liquid level have been simulated: 40 % and 60 %. Comparing Figure 4.13 and 4.15, which have the same amount of mass, it is possible to see not too much differences. Amplitude of yaw rates for both tractor and trailer are slightly under estimated, but the trend is quite comparable. It can be observed that there are no substantial changes between rigid and liquid load, meaning that lateral sloshing is not influencing too much vehicle dynamics, at least in the early phase, during when rear axle starts to slip. Sloshing motion seems to influence tractor and trailer yaw rate only after the jack-knife has occurred.

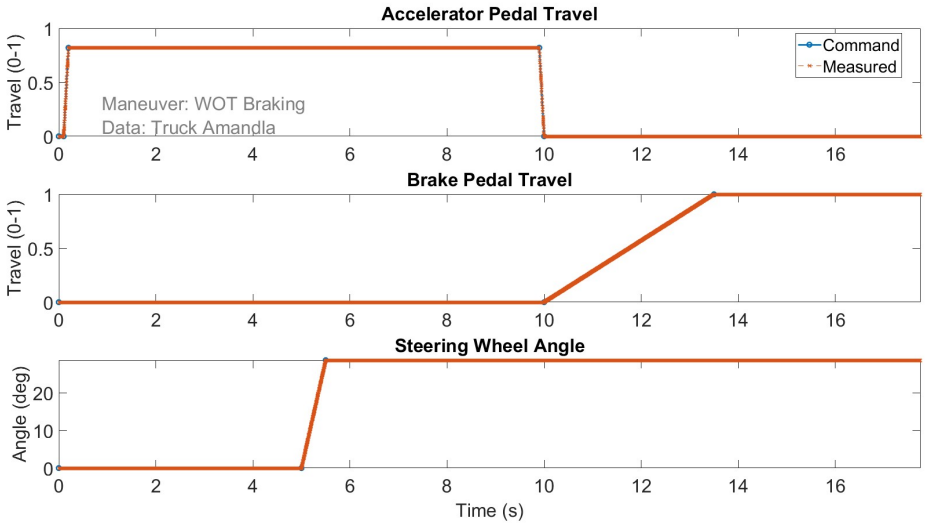

Figure 4.14: Driver's input during jack-knife manoeuvre.

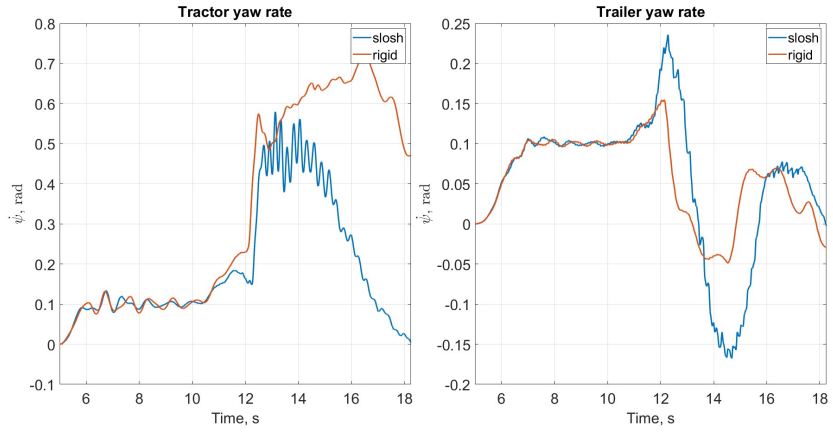

Figure 4.15: Yaw rate during steering and braking only with rear axle when tank is filled at 40 %.

Similar things can be said also in the case of 60 % filling level (Figure 4.16), where the differences between rigid and sloshing load are even lower also after the complete rear axle slippage.

4.4.2 Jack-knife with longitudinal sloshing

More interesting analysis is the study of jack-knife due to longitudinal sloshing. Due to model definition, it can be used only in manoeuvres which does not involve

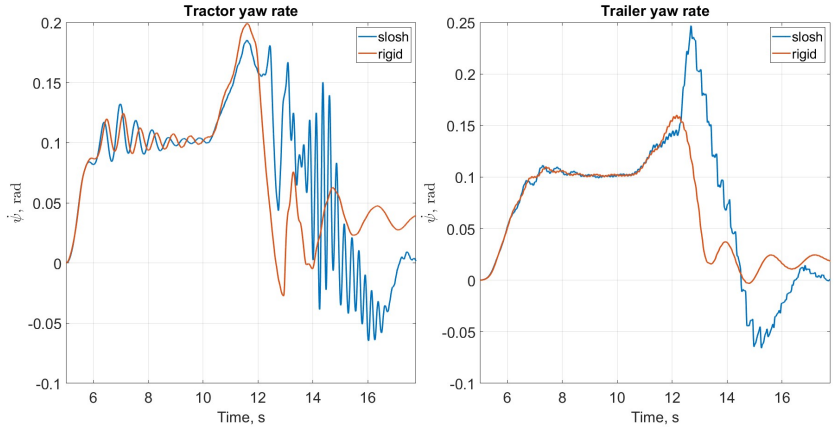

Figure 4.16: Yaw rate during steering and braking only with rear axle when tank is filled at 60 %.

lateral dynamic. For this reason the manoeuvre is equal to the one described with lateral sloshing, but this time no steer input is applied.

This time, the sloshing have a great impact on vehicle behaviour and it can be observed looking at Figures 4.17 through 4.22. The jack-knife phenomenon is influenced greatly in both magnitude and timing. Sloshing seems to delay the moment of jack-knife but, looking at yaw rates it also develops in abrupt way. In fact, the presence of sloshing load increases the yaw rate faster than rigid load. The difference in timing can be due to delay in sloshing motion and when the sloshing mass approaches the front tank wall, the vehicle becomes unstable since a great amount of fluid moves on tractor rear axle.

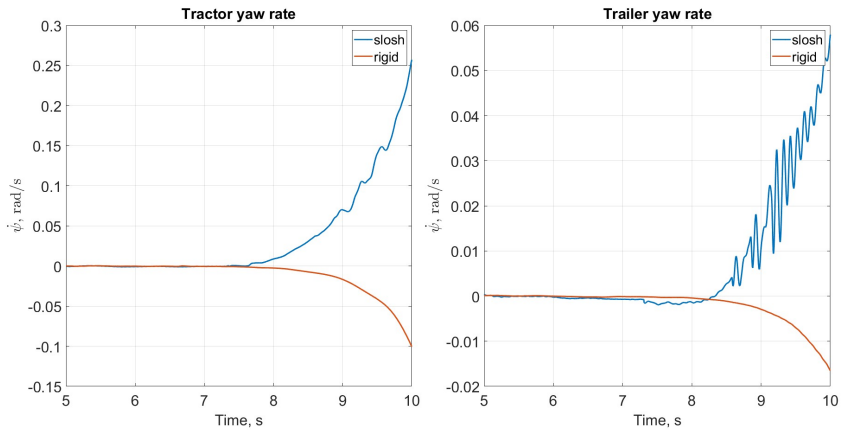

Figure 4.17: Yaw rate when braking only with rear axle when tank is filled at 40 %.

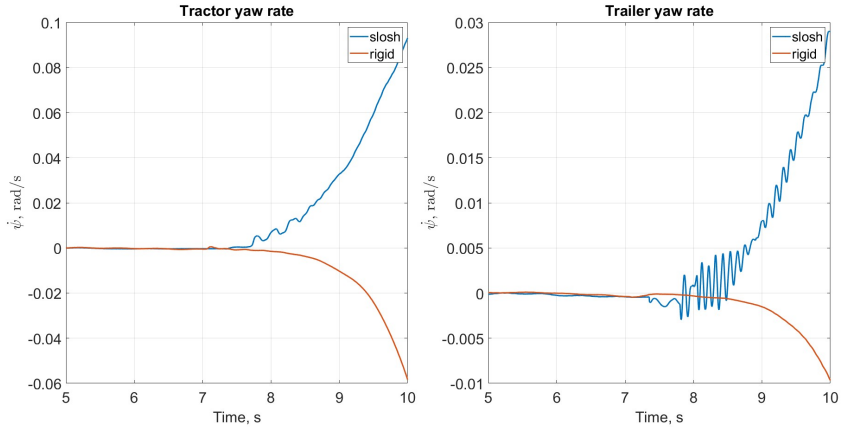

Figure 4.18: Yaw rate when braking only with rear axle when tank is filled at 50 %.

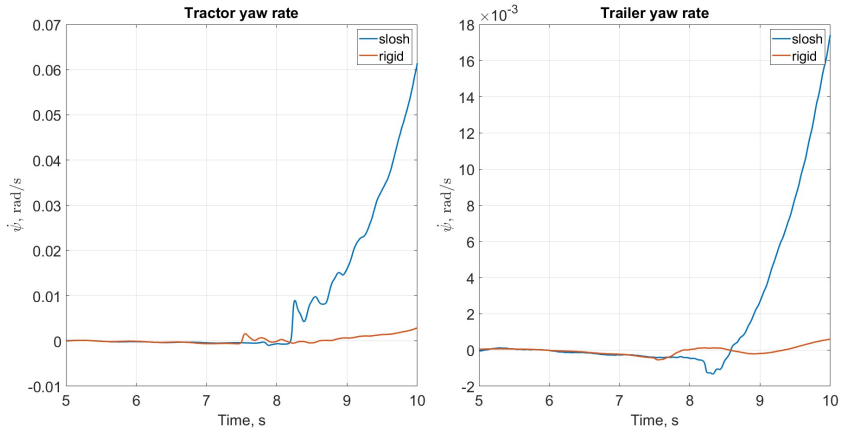

Figure 4.19: Yaw rate when braking only with rear axle when tank is filled at 70 %.

An other possible observation can be done looking at what happens changing liquid fill percentage. While the jack-knife seems not so influenced by the amount of rigid load, it changes noticeably when vehicle carries liquid. In fact, changing the liquid level, it is possible to notice that jackknifing with rigid load changes just a little bit in intensity and timing, contrarily to sloshing load. In case of 40 % (Figure 4.17) the sloshing mass is the greatest part of the total payload, this develops great forces in longitudinal direction and increases the vertical load on tractor rear axle, which leads to locking and consequently to jack-knife. In the high filling level (Figure 4.19), there is a relatively higher amount of fixed mass than sloshing one, anyway the absolute value of oscillating mass is still bigger than

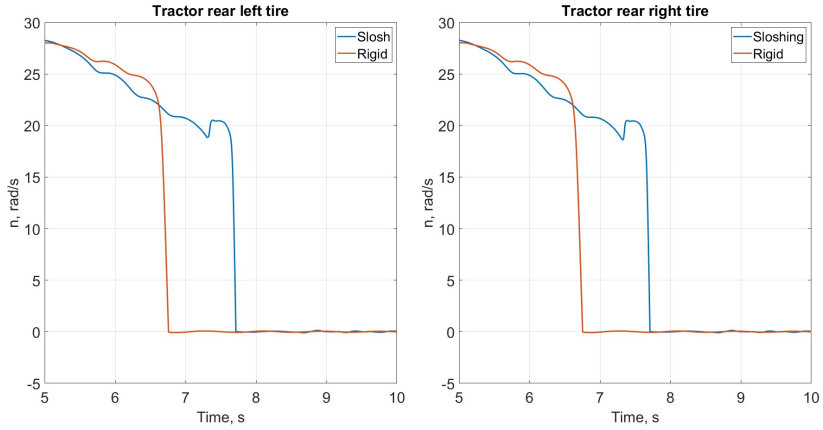

Figure 4.20: Tires speed when tank is filled at 40 % while braking.

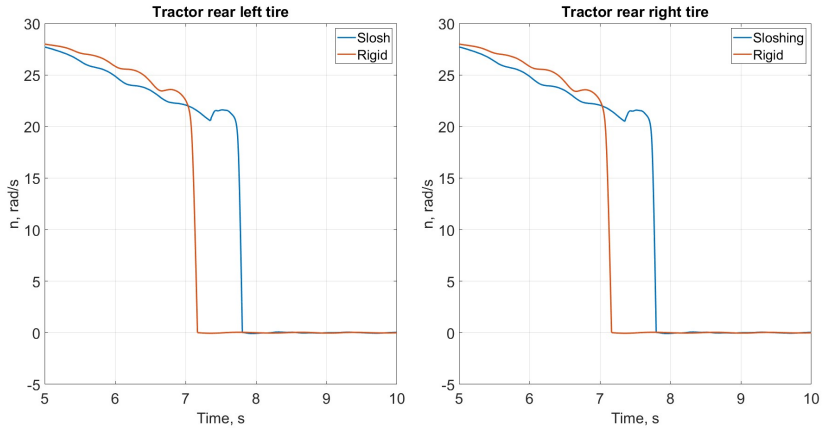

Figure 4.21: Tires speed when tank is filled at 50 % while braking.

in 40 % case. This explains why jack-knife event happens more delayed. In the intermediate level (Figure 4.18), a significant decrease in yaw rates can be observed with respect to lower fill level. This can be explained looking at trailer pitch angle, at Figures 4.23, 4.24 and 4.25. It is possible to see a significant difference when the tank liquid level is low. In fact, simulation at 40 % showed a lift of trailer axle due to pendulum model. In reality this event does not happens, so these results may be affected by the kind of model. Increasing the payload the pitch angle decrease and should lead to less jack-knifing problems. However, as said before, the absolute amount of sloshing mass is increasing and this still contributes to jack-knife.

Summing up the results in Figures 4.26, 4.27 and4.28, it is possible to observe a correlation between jack-knife and liquid filling level. As far as the level increases, sloshing load tens to become similar to a rigid one and the instability related to

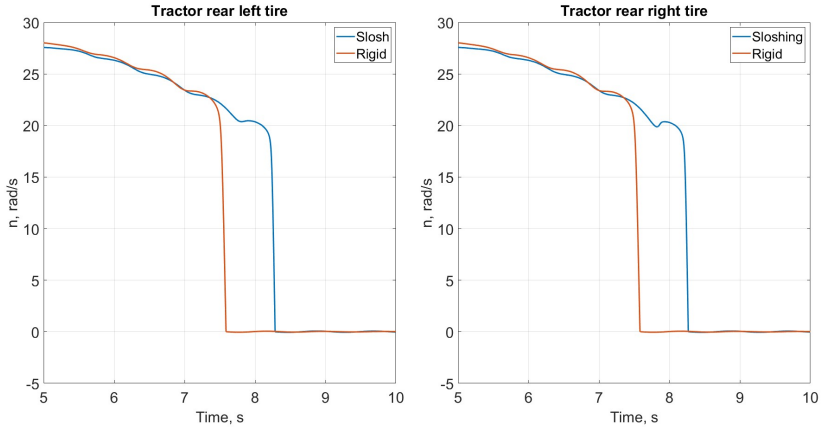

Figure 4.22: Tires speed when tank is filled at 70 % while braking.

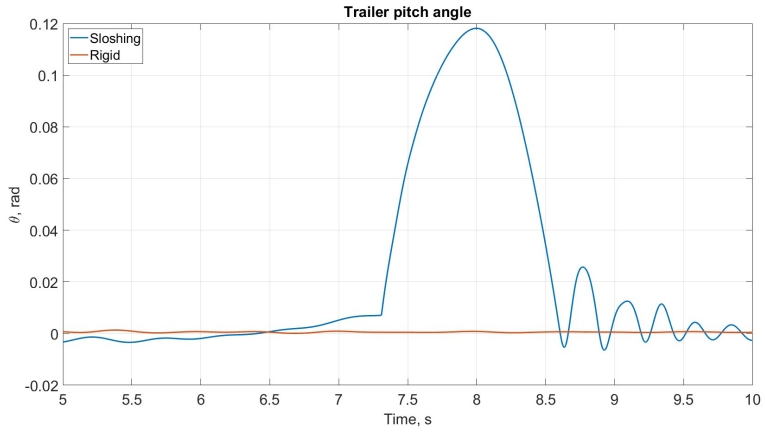

Figure 4.23: Trailer pitch angle when tank is filled at 40 % while braking.

heavy braking has becomes less problematic.

Common solution to limit the jack-knife problem are usually related to hitch. Sometimes a constraint to the max angle can be applied when the vehicle is in motion, while in other cases a damping can be introduced, as shown in [19].

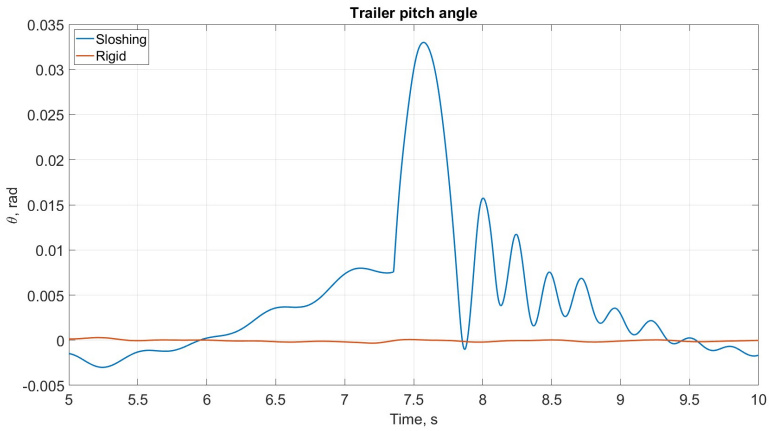

Figure 4.24: Trailer pitch angle when tank is filled at 50 % while braking.

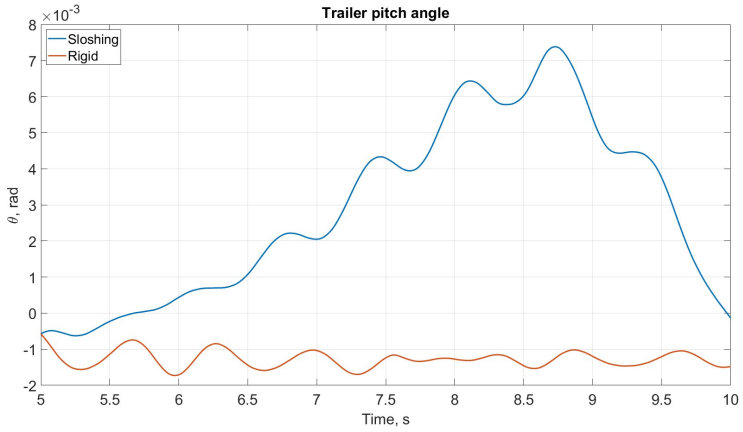

Figure 4.25: Trailer pitch angle when tank is filled at 40 % while braking.

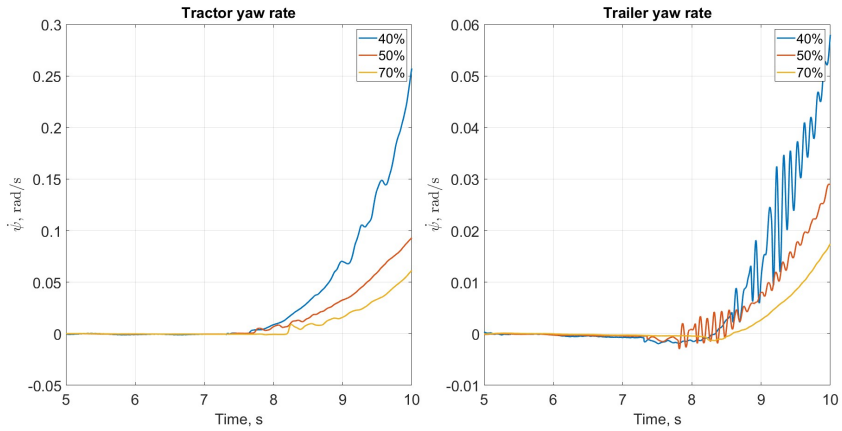

Figure 4.26: Vehicle's and trailer's yaw rate at different liquid filling levels.

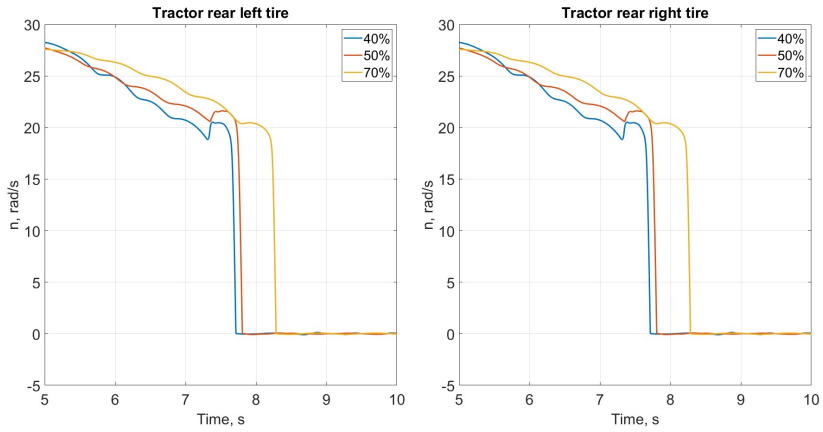

Figure 4.27: Tractor rear wheels speed at different liquid filling levels.

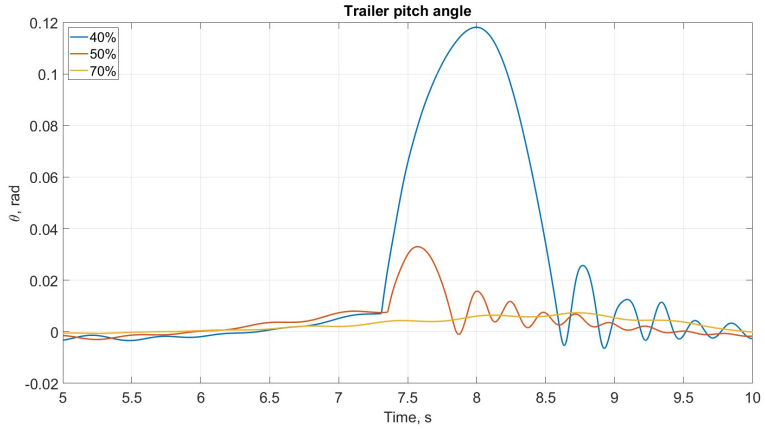

Figure 4.28: Trailer's pitch angle at different liquid filling levels.

Chapter 5

Conclusions

This thesis showed how a relatively simple can be to simulate sloshing phenomenon through Simscape. The basic model implemented for this kind of analysis is quite simple, but with proper modifications it can be adapted to more complex analysis. Sloshing event can be really dangerous in real environment and numerous analysis should be done to improve the knowledge about this problem. Simscape revealed to be a useful tool to study this particular phenomenon with a relatively low amount of time and computational effort. In fact, sloshing fluids require complex fluid-dynamic analyses, but thanks to equivalent mechanical models they can be simplified and easily simulated. Study of sloshing through mechanical models seemed to be quite valid in first approximation, especially for what concerns lateral dynamic. Since pendulum model requires few parameters modification it can be a good approach to simulate fluid complex problem like this. Instead, considering longitudinal sloshing, it seems to be not so valid as for lateral one. This is mainly due to tank's geometry, but it provides a good approximation to set the problem. Moreover, it allowed to understand the influence of sloshing also in presence of jack-knife. In fact, it usually is less studied than overturning but it can lead to serious risk as well.

In order to proper validate the model, only few and simple manoeuvres have been considered, but the possibility to define any type of custom road makes *Simscape Vehicle Templates* a very powerful instrument. In fact, together with the possibility to select a closed loop driver model, almost limitless kind of manoeuvre can be simulated. For example, during model inspections, the possibility to include a banked road has been detected. Moreover, the availability of different models and trailers allows to study vehicles dynamic with a simple approach.

Appendix A

Nomenclature

$a^*_{f/r,i}$	Longitudinal distance to axle, measured backwards from front axle (tractor), or from front articulation point (trailer)
$b_{f,i}$	Longitudinal distance to articulation point, measured forwards from centre of sprung mass
$b'_{f,i}$	Longitudinal distance to front axle (tractor) or to articulation point (trailer), measured forwards from centre of total mass
$b^*_{r,i}$	Longitudinal distance to rear articulation point, measured backwards from front axle
c_1, c_2	Tire constants
$C_{i,f/r}$	Axle cornering stiffness
g	Gravity acceleration
$h_{ar,i}$	Height of articulation point, measured upwards from ground
h_{CM}	Height of total centre of mass, measured upwards from ground
h_{fix}	Distance between fixed mass centre of gravity and roll axis
h_{liq}	Distance between liquid centre of mass and roll axis
$h_{s,i}$	height of centre of sprung mass, measured upwards from ground
$h_{u,i}$	Height of centre of unsprung mass, measured upwards from ground
$I_{i,xx}$	Roll moment of inertia of sprung mass, measured about sprung centre of mass
$I'_{i,xx}$	Roll moment of inertia of sprung mass, measured about origin of (x',y',z') coordinate system

$I_{i,xz}$	Yaw-roll moment of inertia of sprung mass, measured about sprung centre of mass
$I'_{i,xz}$	Yaw-roll moment of inertia of sprung mass, measured about origin of (x',y',z') coordinate system
$I_{i,zz}$	Yaw moment of inertia of sprung mass, measured about sprung centre of mass
$I'_{i,zz}$	Yaw moment of inertia of sprung mass, measured about origin of (x',y',z') coordinate system
$k_{i,f/r}$	Suspension roll stiffness
$k_{t,i}$	Tyres roll stiffness
k_{φ}	Vehicle coupling roll stiffness
L	Tank's length
$L_{i,f/r}$	Suspension roll damping rate
m_i	Total mass
m_{liq}	Liquid mass in the tank
$m_{s,i}$	Sprung mass
$m_{uf,i}$	Unsprung mass of i axle
r_i	Height of roll axis, measured upwards from ground
R	Tank's radius
U	Vehicle's longitudinal velocity
W	Axle weight
β	Side-slip angle
δ	Steering angle
ζ	Pendulum's damping ratio
θ	Pendulum's oscillation angle
λ	Ratio of tank's width to its length
μ	Fluid dynamic viscosity
ν	Fluid kinematic viscosity
ρ	Fluid density
ϕ	Roll angle
ψ	Yaw angle

Appendix B

Vehicle data for lateral sloshing

B.1 Tractor

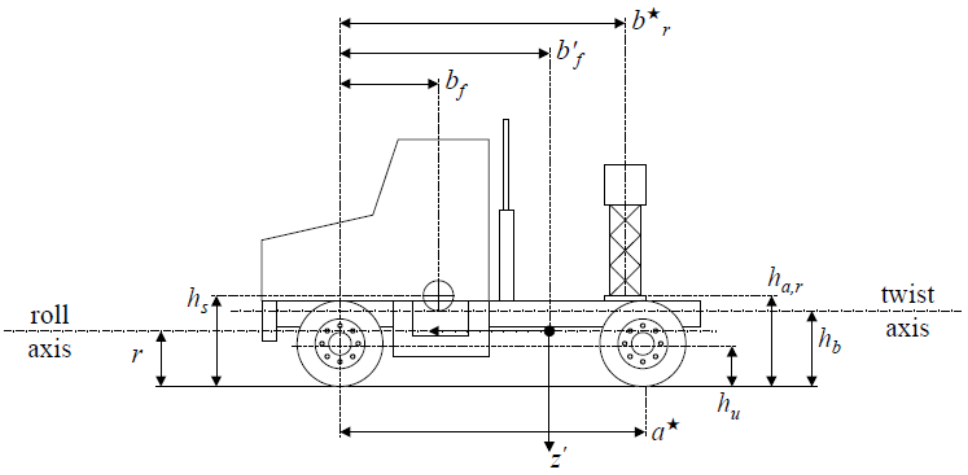

Figure B.1: Tractor scheme, [11].

Table B.1: Main tractor parameters settings.

Parameter	Value	Units	Description
m_s	4819	kg	Sprung mass
$\begin{bmatrix} I_{xx} & I_{xy} & I_{xz} \\ I_{xy} & I_{yy} & I_{yz} \\ I_{xz} & I_{yz} & I_{zz} \end{bmatrix}$	$\begin{bmatrix} 2411 & 0 & 1390 \\ 0 & 0 & 0 \\ 1390 & 0 & 11383 \end{bmatrix}$	kgm^2	Inertia tensor of vehicle
m_u	706	kg	Front axle mass
I_{xx}	440	kgm^2	Front axle roll moment of inertia
I_{zz}	440	kgm^2	Front axle yaw moment of inertia
m_u	1000	kg	Rear axle mass
I_{xx}	563	kgm^2	Rear axle roll moment of inertia
I_{zz}	563	kgm^2	Rear axle yaw moment of inertia
K_h	300×10^3	N/m	Front/rear suspension heave stiffness
L_h	2000	Ns/m	Front/rear suspension heave damping
K_r	380×10^3	Nm/rad	Front suspension roll stiffness
L_r	4.05×10^3	Nms/rad	Front suspension roll damping
K_r	684×10^3	Nm/rad	Rear suspension roll stiffness
L_r	6.68×10^3	Nms/rad	Rear suspension roll damping
K_φ	$3{,}000 \times 10^3$	Nm/rad	Hitch roll stiffness
L_φ	0	Nms/rad	Hitch roll damping

Table B.2: Tractor geometry parameters settings.

Parameter	Value	Units	Description
a^*	3.700	m	Longitudinal distance between front and rear axle
b_f	0.742	m	Longitudinal distance between front axle and COG
h_s	1.058	m	Distance of COG from the ground
r	0.621	m	Distance of roll axis from the ground
b_r^*	3.074	m	Longitudinal distance between hitch and front axle
$h_{a,r}$	1.250	m	Distance of hitch from the ground

Table B.3: Tractor's tires settings.

Parameter	Value	Units	Description
c_1	10.34	rad^{-1}	Front/rear tire constant
c_2	-90.09	$\text{MN}^{-1}\text{rad}^{-1}$	Front/rear tire constant
W_f	5691	kg	Front axle weight (50 % filling)
W_r	7526	kg	Rear axle weight (50 % filling)

B.2 Trailer

Table B.4: Main trailer parameters settings.

Parameter	Value	Units	Description
m_s	3020	kg	Sprung mass
$\begin{bmatrix} I_{xx} & I_{xy} & I_{xz} \\ I_{xy} & I_{yy} & I_{yz} \\ I_{xz} & I_{yz} & I_{zz} \end{bmatrix}$	$\begin{bmatrix} 3090 & 0 & 0 \\ 0 & 0 & 0 \\ 0 & 0 & 37545 \end{bmatrix}$	kgm^2	Inertia tensor of vehicle
m'	800	kg	Axle mass
I'_{xx}	564	kgm^2	Axle roll moment of inertia
I'_{zz}	564	kgm^2	Axle yaw moment of inertia
K_h	300×10^3	N/m	Suspension heave stiffness
d_h	15×10^3	Ns/m	Suspension heave damping
K'_r	800×10^3	Nm/rad	Front suspension roll stiffness
d'_r	23.9×10^3	Nms/rad	Front suspension roll damping

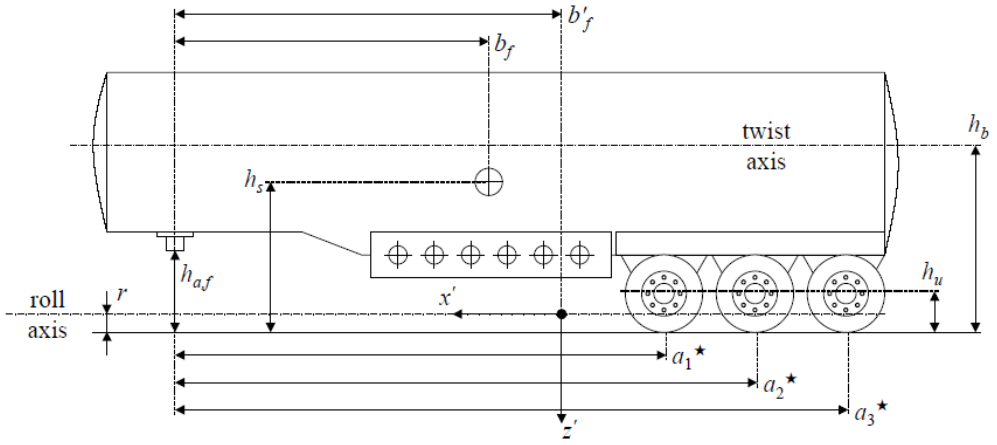

Figure B.2: Trailer scheme., [11]

Table B.5: Trailer geometry parameters settings.

Parameter	Value	Units	Description
a_1^*	6.390	m	Longitudinal distance between hitch and axle 1
a_2^*	7.700	m	Longitudinal distance between hitch and axle 2
a_3^*	9.010	m	Longitudinal distance between hitch and axle 3
b_f	5.494	m	Longitudinal distance between hitch and COG
h_s	1.900	m	Distance of COG from the ground
r	0.100	m	Distance of roll axis from the ground
$h_{a,f}$	1.100	m	Distance of hitch from the ground
h_b	2.050	m	Distance of tank centre to the ground
L	9.5	m	Tank longitudinal length
R	1.15	m	Tank radius

Table B.6: Trailer's tires settings.

Parameter	Value	Units	Description
c_1	9.27	rad^{-1}	Tire constant
c_2	-69.6	$\text{MN}^{-1}\text{rad}^{-1}$	Tire constant
W	6236	kg	Each axle weight (50 % filling)

Appendix C

Vehicle data for longitudinal sloshing

C.1 Tractor

Table C.1: Main tractor parameters settings.

Parameter	Value	Units	Description
m_s	5441	kg	Sprung mass
$\begin{bmatrix} I_{xx} & I_{xy} & I_{xz} \\ I_{xy} & I_{yy} & I_{yz} \\ I_{xz} & I_{yz} & I_{zz} \end{bmatrix}$	$\begin{bmatrix} 10637 & 0 & 13296 \\ 0 & 66480 & 0 \\ 13296 & 0 & 26592 \end{bmatrix}$	kgm^2	Vehicle inertia tensor
m_u	706	kg	Front axle mass
I_{xx}	440	kgm^2	Front axle roll moment of inertia
I_{zz}	440	kgm^2	Front axle yaw moment of inertia
m_u	1000	kg	Rear axle mass
I_{xx}	563	kgm^2	Rear axle roll moment of inertia
I_{zz}	563	kgm^2	Rear axle yaw moment of inertia
$K_{h,f}$	583.73×10^3	N/m	Front suspension heave stiffness
$K_{h,r}$	$1{,}751.2 \times 10^3$	N/m	Rear suspension heave stiffness
$L_{h,f}$	$5.837{,}3 \times 10^3$	Ns/m	Front suspension heave damping
$L_{h,r}$	$1.459{,}3 \times 10^4$	Ns/m	Rear suspension heave damping
$K_{roll,f}$	$2.169{,}2 \times 10^5$	Nm/rad	Front suspension roll stiffness
L_r	$2.169{,}2 \times 10^3$	Nms/rad	Front suspension roll damping
K_r	$6.507{,}6 \times 10^5$	Nm/rad	Rear suspension roll stiffness
L_r	$5.423{,}0 \times 10^3$	Nms/rad	Rear suspension roll damping
K_φ	$3{,}000 \times 10^3$	Nm/rad	Hitch roll stiffness
L_φ	0	Nms/rad	Hitch roll damping

Table C.2: Tractor geometry parameters settings.

Parameter	Value	Units	Description
a^*	3.5052	m	Longitudinal distance between front and rear axle
b_f	1.7374	m	Longitudinal distance between front axle and COG
h_s	1.0363	m	Distance of COG from the ground
r	0.0305	m	Distance of roll axis from the ground
b_r^*	2.9566	m	Longitudinal distance between hitch and front axle
$h_{a,r}$	0.9754	m	Distance of hitch from the ground
T	1.006	m	Track width

C.2 Trailer

Table C.3: Main trailer parameters settings.

Parameter	Value	Units	Description
m_s	$1.696{,}1 \times 10^3$	kg	Sprung mass
$\begin{bmatrix} I_{xx} & I_{xy} & I_{xz} \\ I_{xy} & I_{yy} & I_{yz} \\ I_{xz} & I_{yz} & I_{zz} \end{bmatrix}$	$\begin{bmatrix} 3090 & 0 & 0 \\ 0 & 0 & 0 \\ 0 & 0 & 37545 \end{bmatrix}$	kgm^2	Inertia tensor of vehicle
m'	800	kg	Axle mass
I'_{xx}	564	kgm^2	Axle roll moment of inertia
I'_{zz}	564	kgm^2	Axle yaw moment of inertia
K_h	$1.751{,}2 \times 10^6$	N/m	Suspension heave stiffness
d_h	$1.459{,}3 \times 10^4$	Ns/m	Suspension heave damping
K'_r	$6.507{,}6 \times 10^5$	Nm/rad	Front suspension roll stiffness
d'_r	$5.423{,}0 \times 10^3$	Nms/rad	Front suspension roll damping

Table C.4: Trailer geometry parameters settings.

Parameter	Value	Units	Description
a^*	10.0584	m	Longitudinal distance between hitch and axle
b_f	5.1816	m	Longitudinal distance between hitch and COG
h_s	1.4326	m	Distance of COG from the ground
r	0.100	m	Distance of roll axis from the ground
$h_{a,f}$	0.9754	m	Distance of hitch from the ground
h_b	2.050	m	Distance of tank centre to the ground
L	10	m	Tank longitudinal length
R	1.015	m	Tank radius

Bibliography

[1] *Veicoli coinvolti in incidenti stradali*. 2021. URL: `http://dati.istat.it` (cit. on p. 1).

[2] Shahrouz Aliabadi, Andrew Johnson, and Jalal Abedi. «Comparison of finite element and pendulum models for simulation of sloshing». eng. In: *Computers and fluids* 32.4 (2003), pp. 535–545. ISSN: 0045-7930 (cit. on pp. 2, 4, 5, 9, 13).

[3] Luca Guagliumi, Alessandro Berti, Eros Monti, and Marco Carricato. «A Simple Model-Based Method for Sloshing Estimation in Liquid Transfer in Automatic Machines». eng. In: *IEEE access* 9 (2021), pp. 129347–129357. ISSN: 2169-3536 (cit. on pp. 3–5).

[4] Xian-sheng Li, Xue-lian Zheng, Yuan-yuan Ren, Yu-ning Wang, and Zhu-qing Cheng. «Study on Driving Stability of Tank Trucks Based on Equivalent Trammel Pendulum for Liquid Sloshing». eng. In: *Discrete dynamics in nature and society* 2013 (2013), pp. 1–15. ISSN: 1026-0226 (cit. on p. 6).

[5] Bernhard Godderidge, Stephen R. Turnock, and Mingyi Tan. «A rapid method for the simulation of sloshing using a mathematical model based on the pendulum equation». eng. In: *Computers and fluids* 57 (2012), pp. 163–171. ISSN: 0045-7930 (cit. on pp. 7, 39).

[6] Xue-lian Zheng, Hao Zhang, Yuan-yuan Ren, Ze-hong Wei, and Xi-gang Song. «Rollover stability analysis of tank vehicles based on the solution of liquid sloshing in partially filled tanks». eng. In: *Advances in mechanical engineering* 9.6 (2017), pp. 168781401770389–. ISSN: 1687-8132 (cit. on pp. 7, 8, 19).

[7] «Investigation of sloshing effects on lateral stability of tank vehicles during turning maneuver». eng. In: *Mechanics based design of structures and machines* 50.9 (2022), pp. 3180–3205. ISSN: 1539-7734 (cit. on pp. 9–12).

[8] Dušan Žagar Vesna Vidmar Gregor Petkovšek. «Simulation of fluid sloshing in a tank unsing the SPH and pendulum methods». eng. In: *ACTA hydrotechnica* (2018) (cit. on pp. 11, 13–15).

[9] Lennart Strandberg. *Lateral stability of road tankers: Vol 1. Main report. (with Swedish summary: Tankfordons sidstabilitet)*. eng. VTI rapport. 1978.

[10] Lennart Strandberg. *Lateral stability of road tankers: Vol. 2 Appendices*. eng. VTI rapport. 1978 (cit. on p. 15).

[11] David John Matthew Sampson. «Active roll control of articulated heavy vehicles». PhD thesis. University of Cambridge UK, 2000 (cit. on pp. 16, 25, 62, 65).

[12] Shahram Azadi, Ali Jafari, and Masoud Samadian. «Effect of parameters on roll dynamic response of an articulated vehicle carrying liquids». eng. In: *Journal of mechanical science and technology* 28.3 (2014), pp. 837–848. ISSN: 1738-494X (cit. on pp. 16, 23–25).

[13] Norman H. Abramson and Norman H. Abramson. *The dynamic behavior of liquids in moving containers : with applications to space vehicle technology / ed. H. Norman Abramson*. eng. NASA SP. Washington: NASA, 1966 (cit. on pp. 20, 36, 39, 42).

[14] Mohammad Mahdi Jalili, Mehrdad Motavasselolhagh, Rouhollah Fatehi, and Mohammad Sefid. «Investigation of sloshing effects on dynamic response of an articulated vehicle carrying liquids». eng. In: *Proceedings of the Institution of Mechanical Engineers. Part D, Journal of automobile engineering* 232.10 (2018), pp. 1385–1401. ISSN: 0954-4070 (cit. on pp. 37–39).

[15] G Yan and S Rakheja. «Straight-line braking dynamic analysis of a partly filled baffled and unbaffled tank truck». eng. In: *Proceedings of the Institution of Mechanical Engineers. Part D, Journal of automobile engineering* 223.1 (2009), pp. 11–26. ISSN: 0954-4070 (cit. on pp. 38, 40, 41).

[16] Yuchun Li and Jinting Wang. «A supplementary, exact solution of an equivalent mechanical model for a sloshing fluid in a rectangular tank». eng. In: *Journal of fluids and structures* 31 (2012), pp. 147–151. ISSN: 0889-9746 (cit. on p. 39).

[17] R Ranganathan, Y Ying, and JB Miles. *Development of a mechanical analogy model to predict the dynamic behavior of liquids in partially filled tank vehicles*. Tech. rep. SAE Technical Paper, 1994 (cit. on pp. 42, 43).

[18] Korang Modaressi-Tehrani, S. Rakheja, and I. Stiharu. «Three-dimensional analysis of transient slosh within a partly-filled tank equipped with baffles». eng. In: *Vehicle system dynamics* 45.6 (2007), pp. 525–548. ISSN: 0042-3114 (cit. on pp. 44, 45, 47).

[19] Edwin Charles Mikulcik. «The dynamics of tractor-semitrailer vehicles: The Jackknifing Problem». In: *SAE Transactions* (1971), pp. 154–168 (cit. on pp. 49, 50, 55).